The Effect of Sea Spray Evaporation on Tropical Cyclone Boundary Layer Structure and Intensity*

YUQING WANG

International Pacific Research Center, School of Ocean and Earth Science and Technology, University of Hawaii at Manoa, Honolulu, Hawaii

JEFF D. KEPERT AND GREG J. HOLLAND

Bureau of Meteorology Research Centre, Melbourne, Victoria, Australia

(Manuscript received 1 June 2000, in final form 8 April 2001)

ABSTRACT

Strong winds in a tropical cyclone over the ocean can produce high seas with substantial amounts of spray in the lower part of the atmospheric boundary layer. The effects that the evaporation of this sea spray may have on the transfer of energy between the ocean and the atmosphere, and consequent effects on the boundary layer structure, cumulus convection, and the evolution of the tropical cyclone, are largely unknown. In this study, a high-resolution tropical cyclone model with explicit cloud microphysics, developed by Y. Wang, has been used to study these potential effects. The sea spray evaporation is incorporated into the model by two bulk parameterization schemes with quite different properties.

The numerical results show that inclusion of the Fairall et al. sea spray parameterization increases the direct sensible heat flux from the ocean by about 70%, but has little effect on the direct latent heat flux. Sea spray itself causes a sensible heat flux of only about 6% of the direct sensible heat flux, while it contributes a latent heat flux by evaporation of sea spray droplets by 60%–70% of the direct latent heat flux. As a result, the total enthalpy flux with sea spray evaporation increases by about 20%, while the net contribution by sea spray is only about 1.5% of the total enthalpy flux. Consistent with this, the intensity of the model tropical cyclone is moderately increased by 8% in the maximum wind speed by the introduction of sea spray. The lower atmosphere becomes cooler and moister due to the evaporation of sea spray, which is supported by the available observations. The cooling in the surface layer further modifies the boundary layer structure and the activity of convection, especially in the near-core region where the highest concentration of sea spray exists.

On the other hand, with the Andreas and DeCosmo parameterization scheme, the intensity of the model tropical cyclone is increased by 25% in maximum wind speed. This dramatic increase in the model tropical cyclone intensity is due to both the large net sensible heat flux and the latent heat flux associated with the effect of sea spray by this parameterization scheme. The net upward sensible heat flux warms the air near the surface and results in a near-isothermal surface layer in the near-core environment under the tropical cyclone. Such a structure, however, is not supported by the available observations, which the authors argue is not physically realistic. The radically different results with this scheme are due to the unusual way that the feedbacks between direct and spray-mediated fluxes are handled within the parameterization.

1. Introduction

Strong winds in severe weather systems, such as tropical cyclones, over the open ocean can generate substantial amounts of sea spray into the lowest few meters of the atmosphere by both bursting air bubbles in whitecaps and whipping spume from the tips of waves. Speculation as to the possible role of sea spray in enhancing air–sea fluxes has a long history reaching back at least to Ling and Kao (1976), although there is still no unequivocal answer. Excellent recent reviews of sea spray physics may be found in Andreas et al. (1995) and Mestayer et al. (1996). Tropical cyclones are known to be fueled by the energy extracted from the ocean, and the maximum potential intensity (MPI) theories of Emanuel (1986, 1991) and Holland (1997) have substantial predictive skill. They both, however, rely on assumptions about the air–sea temperature difference and boundary layer relative humidity without considering the processes that determine them. In this sense, they must therefore be regarded as incomplete. Indeed, Emanuel

* School of Ocean and Earth Science and Technology Contribution Number 5630, International Pacific Research Center Contribution Number IPRC-93.

Corresponding author address: Dr. Yuqing Wang, IPRC/SOEST, University of Hawaii at Manoa, 2525 Correa Road, Honolulu, HI 96822.
E-mail: yqwang@soest.hawaii.edu

and Holland consider both the air–sea temperature difference and boundary layer relative humidity as tuning parameters, and Holland (1997) gives an analysis that shows that the MPI is quite sensitive to each of these in both his and Emanuel's models.

However, interest in sea spray evaporation in tropical cyclones goes back further than this. Anthes (1982) proposed that evaporation of sea spray would produce a strong cooling in the layer of air within a meter or so of the ocean's surface, and thus would enhance the sensible heat transfer and strengthen the storm. Betts and Simpson (1987) considered simultaneous heat and moisture budgets within a subcloud column of air as it spiraled inward from 150- to 30-km radius in a hurricane. They found that it was necessary to include a droplet evaporation process to close the budget, although they were unable to separate the effects of sea spray and rain evaporation.

In the context of spray evaporation producing near-surface cooling, highly interesting observations were taken by an oceanographic research vessel of the former Soviet Union during Typhoons Skip and Tess in November 1988 over the western North Pacific. These show a significant increase of the marine boundary layer cooling with increasing wind speeds (Korolev et al. 1990), and that in the lowest several hundred meters of the atmosphere, the air–sea temperature difference can be as large as 4°–6°C in strong tropical cyclones as wind speeds rise above 25 m s^{-1}. Such a large cooling in the tropical cyclone boundary layer cannot be explained solely by the adiabatic cooling associated with the low pressure in the cyclone core, nor by the evaporation of falling rain, because the cooling did not only cover the core region but was also found in a cloud-free region with gale force winds. It was therefore suggested that this reduction in surface air temperature primarily occurred due to evaporation of sea spray (Korolev et al. 1990; Pudov and Holland 1994).

A subsequent, more extensive, study by Cione et al. (2000) used data from buoys and coastal stations. They confirmed the increase in air–sea temperature difference, but found that the bulk of the cooling occurred as the inwardly spiraling boundary layer air was between 150 and 300 km from the cyclone center, where the air–sea temperature difference increased from less than 0.5 K to around 2.5 K. The air–sea temperature difference was essentially constant farther inward. They also analyzed a smaller amount of humidity data, and found evidence of drying outside the core, with a weak minimum in the specific humidity at a radius of about 200 km. Since this was coincident with the band of cooling, they concluded that the source of the cooling was convective downdrafts, rather than sea spray evaporation.

Prompted partly by the former set of observed air–sea temperature differences, and building on improved knowledge of droplet behavior flowing from the Humidity Exchange over the Sea program (HEXOS; Katsaros et al. 1987), Fairall et al. (1994, henceforth FKH) developed a bulk parameterization of spray-mediated fluxes, which is the first parameterization to be considered here. They incorporated this into a simple slab boundary layer model and showed that the inclusion of spray evaporation produced a more realistic boundary layer with air–sea temperature differences more consistent with the observations. Subsequent extension of this model by Kepert and Fairall (1999) to include the effects of rain evaporation and cloud downdrafts confirmed this result. A key property of the FKH parameterization is that its effect is largely to redistribute the total enthalpy flux between its latent and sensible components. This is supported by numerical spray droplet models (e.g., Rouault et al. 1991; Edson et al. 1996; Kepert et al. 1999), which show that evaporation of sea spray mainly plays a role in redistributing sensible and latent heat fluxes in the marine boundary layer rather than altering the net enthalpy flux.

Direct measurements of air–sea thermodynamic fluxes become extremely difficult at high wind speeds, and so far are limited to 23 m s^{-1} for sensible heat, and 18 m s^{-1} for moisture. Both these records were achieved during the HEXOS main experiment, conducted on a platform in 18-m-deep water off the Dutch coast in 1986 (Katsaros et al. 1987). The initial analysis of these data (DeCosmo et al. 1996) found no signature due to sea spray, and concluded that the spray-mediated fluxes were either negligible under those conditions, or were masked by negative feedbacks. However, a recent reanalysis of this data, which claims to find a clear signature (Andreas and DeCosmo 1999), resulted in the second spray parameterization considered here. This parameterization, although based on similar physics and some of the same observations as those of FKH, differs markedly in that it produces very large perturbations to the total enthalpy flux. We will discuss its properties in more detail below.

Several earlier studies have considered whether the presence of sea spray can affect the tropical cyclone intensity. Lighthill et al. (1994) and Henderson-Sellers et al. (1998) suggested that evaporation of sea spray would provide a self-limiting process for tropical cyclone intensity. They argued that the energy input per unit mass of air would be reduced if air at the eyewall base is well below the underlying sea surface temperature due to the evaporative cooling by sea spray. On the other hand, Emanuel (1995a) assumed that since the evaporation of sea spray does not significantly affect the enthalpy flux at the sea surface and scarcely changes the thermodynamic efficiency of the energy input and, thus, argued that it would not limit or affect the maximum achievable intensity of a tropical cyclone.

More recently, attention has been given to the quantitative evaluation of the effect of sea spray on intensity of tropical cyclones using numerical models, with contrasting results. Andreas and Emanuel (1999) reconsidered spray droplet microphysics and, using the Andreas

and DeCosmo (1999) parameterization, showed that the evaporation of sea spray increases the maximum potential intensity. Using the FKH bulk parameterization scheme for spray-mediated fluxes in an air–sea coupled model, Bao et al. (2000) also found a significant increase in both intensification rate and the peak intensity in a case study of Hurricane Opal. In contrast, Wang et al. (1999) and Uang (1999) reported a reduction of the model cyclone intensification rate but with little effect on the final intensity, in idealized studies using the FKH parameterization. Their results also showed the potential sensitivity of the effect of sea spray to the initial conditions of the numerical models. Since these studies used either different parameterization schemes for sea spray or different model settings, direct comparison is impossible and thus more extensive studies in just one model framework with same settings will help clarify the potential effect of sea spray on tropical cyclones.

In this study, a high-resolution tropical cyclone model with explicit cloud microphysics developed by Wang (1999) is used to study how and to what degree the sea spray evaporation can affect both the boundary layer structure, and the intensity of a tropical cyclone by modifying the heat fluxes at the sea surface. The sea spray evaporation is incorporated into the model by either the bulk parameterization scheme derived by FKH, or by a streamlined version of the Andreas and DeCosmo (1999) scheme, which will be developed below. We will show that inclusion of the former parameterization generally has a moderate effect on intensity and boundary layer structure of a model tropical cyclone. On the other hand, the latter parameterization has a dramatic effect that we will argue is physically unrealistic. In the next section we will summarize the numerical model used in this study and give brief summaries of the respective spray parameterizations. Design of the numerical experiments is presented in section 3, while results are discussed in detail in section 4. The last section summarizes our major findings and discusses further research directions on this topic.

2. The numerical model

a. Model framework

The numerical model used in this study is the triply nested movable mesh, high-resolution tropical cyclone model (TCM3) developed by Wang (1999). The model is formulated in Cartesian coordinates in the horizontal and σ (pressure normalized by surface pressure) coordinates in the vertical. The current version of the model assumes hydrostatic balance; however, nonhydrostatic effects are not expected to alter the conclusions of this study. The model consists of 20 layers in the vertical from $\sigma = 0$ to 1 with higher resolution in the planetary boundary layer. The layer interfaces are placed at $\sigma =$ 0.0, 0.04, 0.07, 0.09, 0.11, 0.14, 0.17, 0.21, 0.27, 0.35, 0.45, 0.55, 0.65, 0.74, 0.82, 0.88, 0.93, 0.96, 0.984, 0.994, and 1.0, giving a substantial concentration of resolution within the boundary layer.

TABLE 1. Summary of the grid system of the triply nested movable mesh tropical cyclone model.

Domain	Dimensions (x, y)	Grid size (km)	Time step (s)
Mesh A	141 × 121	45	450
Mesh B	103 × 103	15	150
Mesh C	109 × 109	5	50

A two-way interactive, triply nested movable mesh technique is used so that high resolution can be achieved in the cyclone core region. Table 1 gives the specified domain size, resolution, and time step for each mesh domain. The outermost mesh A is fixed with an open lateral boundary conditions in the north and south boundaries, and a cyclic boundary condition in the east–west direction. The size of the domain is chosen sufficiently large so that the influence of the lateral boundary conditions on the evolution of the model tropical cyclone is minimized. The intermediate mesh B is used to capture the synoptic-scale flow associated with a tropical cyclone, and moves following the model tropical cyclone during the course of the time integration. The innermost mesh C with a grid spacing of 5 km is designed to resolve the central core and major spiral rainbands of a tropical cyclone explicitly, and also follows the model tropical cyclone. The mesh movement is automatically determined by an algorithm similar to the one used in the Geophysical Fluid Dynamics Laboratory hurricane model (Kurihara et al. 1998).

The direct surface fluxes are calculated based on the Monin–Obukhov similarity theory. The stability functions for momentum, heat, and moisture are modified for highly unstable conditions as suggested by Fairall et al. (1996). The roughness length for momentum over the ocean is calculated by the Charnock (1955) relationship with a Charnock constant of 0.016 with an additional term added to account for the molecular kinematic viscosity as suggested by Smith (1988), given by

$$z_{0u} = 0.016\frac{u_*^2}{g} + 0.11\frac{\mu}{u_*}, \tag{1}$$

where u^* is the friction velocity, g the gravitational acceleration, and μ the dynamic viscosity of air. The roughness lengths for heat (z_{0T}) and moisture (z_{0q}) are assumed to be constant and given by

$$z_{0T} = \text{Max}(4.9 \times 10^{-5},\ 0.2\mu/u_*), \quad \text{and}$$
$$z_{0q} = \text{Max}(1.3 \times 10^{-4},\ 0.3\mu/u_*). \tag{2}$$

The constants used in (2) are based on Large and Pond (1982) and Miller et al. (1992). Note that a lower bound for either z_{0T} or z_{0q} is assumed so that the roughness length is not allowed to be less than the value corresponding to a smooth surface (Garratt 1992). By using (2), the transfer coefficients for heat (Ch) and moisture

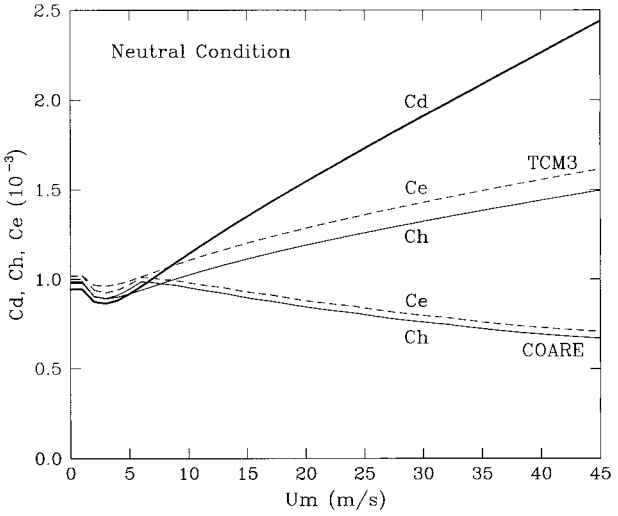

FIG. 1. Comparison of drag coefficient (Cd), exchange coefficients for heat (Ch), and moisture (Ce) as a function of wind speed at 26.5 m above the sea surface under neutral conditions, obtained by the standard TCM3 algorithm (Wang 1999) and by the COARE algorithm (Fairall et al. 1996).

(Ce) within the bulk flux formulas increase with wind speed, but less rapidly than does the drag coefficient (Cd).

Since the exchange coefficients are critical parameters in dealing with air–sea interactions, in Fig. 1 we compare those obtained by the algorithm in our TCM3 with those obtained by the Coupled Ocean–Atmosphere Response Experiment (COARE) algorithm of Fairall et al. (1996) under neutral surface conditions (no air–sea temperature difference). The latter algorithm is used in conjunction with the second sea spray parameterization scheme developed by Andreas and DeCosmo (1999). Note that in order for a direct comparison with our model results, the wind speed in Fig. 1 was determined at the height of 26.5 m above sea surface, equivalent to the height of our lowest model level. We can see from Fig. 1 that our TCM3 algorithm produces the exchange coefficients that increase with wind speed and are much larger than those produced by the COARE algorithm, by which the exchange coefficients slightly decrease with wind speed. The ratio of Ce/Cd at large wind speeds, however, is generally less than 0.7 in our TCM3, and becomes less than 0.3 for wind speeds over 40 m s^{-1} for the COARE algorithm. Based on numerical and theoretical models of tropical cyclones, Emanuel (1995b) suggested that this ratio lies in the range 0.75–1.5 in the high wind conditions of intense tropical cyclones. By our TCM3 algorithm, reasonable intense tropical cyclones can develop with a ratio that can be slightly less than the critical ratio suggested by Emanuel. However, we will show in the next section that the COARE algorithm alone, without the effect of sea spray, can only produce a marginal intense storm in our TCM3.

The turbulent fluxes above the surface layer are calculated based on the so-called E–ϵ turbulence closure scheme, in which both the turbulence kinetic energy (TKE) and its dissipation rate are prognostic variables in the model (Detering and Etling 1985; Langland and Liou 1996). This closure scheme has been found to have many advantages for use in mesoscale numerical models (e.g., Holt et al. 1990; Huang and Raman 1991; Langland and Liou 1996). To better represent the mixing in clouds, the buoyancy production term in both the TKE and its dissipation rate equations in cloud regions is modified to enhance the mixing in clouds according to Durran and Klemp (1982) and Tripoli (1992).

The cloud microphysics are included based on a bulk parameterization scheme. By this approach, we predict mixing ratios of water vapor, rainwater, cloud water, cloud ice, snow, and graupel. The parameterization of cloud microphysics in the model is based on the existing schemes that are extensively tested and used in many other cloud/mesoscale models in recent years (e.g., Lin et al. 1983; Rutledge and Hobbs 1983, 1984; Ikawa and Saito 1991; Reisner et al. 1998). Cloud water is assumed to be monodispersed and to move with the air, while cloud ice is monodispersed but precipitates with the terminal velocity given by Heymsfield and Donner (1990). Condensation (evaporation) of cloud water takes place instantaneously when the air is supersaturated (subsaturated). The sizes of raindrops, snow, and graupel are assumed to be distributed continuously and follow an exponential distribution given by Marshall and Palmer (1948) and Gunn and Marshall (1958). The intercept parameter for rain is taken to be a constant of 1×10^7 m^{-4}, while the intercept parameters for snow and graupel are expressed in terms of their mixing ratios as suggested by Reisner et al. [(1998), as used in the fifth-generation Pennsylvania State University–National Center for Atmospheric Research Mesoscale Model, version 3.2]. The densities for rainwater, snow, and graupel are 10^3, 10^2, and 400 kg m^{-3}, respectively. A full description of the parameterization for cloud microphysics can be found in Wang (1999).

The time integration of the model is accomplished using the leapfrog scheme with intermittent use of the Euler-backward scheme. Each large time step (Δt) of integration consists of one small time step ($\delta t = \Delta t/6$) of one Euler-backward scheme followed by five small time steps of the leapfrog scheme with the standard time filtering to damp the computational mode for the adiabatic component of the model. A physical process stage is performed at the end of the dynamical component with the large time step. Note that in order to prevent a false cascade of energy to grid-scale structure through nonlinear aliasing, the second-order horizontal diffusion terms are included in the adiabatic stage and integrated with small time steps. The finite-difference scheme for the adiabatic core of the model is second order and conserves both mass and energy as proposed by Lilly (1964). The physical stage includes two major processes: vertical diffusion and cloud microphysics. In this

stage, the turbulence fields are updated first by the algorithm suggested by Langland and Liou (1996), then the vertical fluxes of momentum, heat, and moisture are calculated by an implicit scheme. The cloud microphysics is treated by a forward-in-time scheme, except for the precipitation/sedimentation terms, which are integrated by a first-order implicit upwinding scheme.

b. The Fairall et al. spray parameterization

The first bulk parameterization scheme for the sea spray evaporation used in this study is that proposed by FKH. This parameterization builds on earlier work on droplet microphysics and the associated timescales by Andreas (1989, 1992), who adapted cloud microphysics equations to saline droplets. Droplet residence time was parameterized as the time taken for a droplet to fall from the significant wave height back to the mean surface. This is typically much longer than the timescale for temperature adjustment, so droplets are assumed to transfer all their sensible heat instantaneously. On the other hand, the evaporation takes place over a longer timescale and so FKH simplified and integrated the droplet radius evolution equation to determine the amount of water actually evaporated in the time available. The source function of Andreas (1992) was modified and extrapolated to give a wind speed dependence proportional to the whitecap coverage, recognizing the importance of wave breaking processes in spray generation. Finally, they introduced a simple parameterization of the negative feedback due to cooling and moistening of the near-surface layer of the atmosphere, assuming that half of the total heat and moisture transferred from the droplets was actually realized above the droplet evaporation layer, with the remaining proportion being consumed in the negative feedback. Thus a feedback coefficient, estimated to be 0.5, was incorporated into their definition of the sensible and latent heat fluxes due to evaporation of sea spray. Subsequently, Kepert and Fairall (1999) examined this and other assumptions in the parameterization using an explicit droplet transport and evaporation model, and found that the feedback coefficient was about 0.7, but stated that there were sufficient uncertainties remaining in the parameterization, and particularly in the source function, to justify not changing it at this stage. Thus the FKH parameterization for the fluxes of sensible and latent heat due to spray, Q_{SF} and Q_{LF} are given by

$$Q_{SF} = 3.2 \times 10^{-8} u_{10}^{3.4} \gamma(u_{10}) \rho_a C_{pa} (T_s - T_a) \quad \text{and}$$

$$Q_{LF} = 3.6 \times 10^{-9} u_{10}^{5.4} \gamma(u_{10}) \beta(T_a) \rho_a L_e [q_{sat}(T_a) - q]. \quad (3)$$

Here, u_{10} is the wind speed adjusted to the 10-m height above the sea surface, ρ_a the air density in the atmospheric surface layer, C_{pa} the specific heat of air at constant pressure, L_e the latent heat of condensation, q_{sat} the saturation mixing ratio, T_s the sea surface temperature, and T_a and q are air temperature and specific humidity in the lower atmosphere. Spray droplets evaporate at their evaporating temperature T_{ev}, which can be regarded as a wet-bulb temperature modified for the effects of salinity and curvature, and not at the air temperature. Thus Q_{LF} would be expected to be proportional to $q_s(T_{ev}) - q$, rather than $q_s(T_a) - q$ as given. The term

$$\beta(T_a) = \left[1 + \frac{0.622 L_e^2}{R C_{pa} T_a^2} q_s(T_a)\right]^{-1}, \quad (4)$$

where R is the gas constant of dry air, corrects for this. The 10-m wind speed is adjusted to the significant wave height h through the term

$$\gamma(u_{10}) = 1 - 0.087 \ln\frac{10}{h}, \quad (5)$$

while h is given by (Kinsman 1965)

$$h(u_{10}) = 0.015 u_{10}^2. \quad (6)$$

Note that this is appropriate to a fully developed sea and neglects the effects of fetch, which might be expected to be important in tropical cyclones. We argue that this is not a serious omission, as the short, steep waves in a tropical cyclone would be expected to produce greater amounts of spray than a fully developed sea, and the two errors would at least partially cancel. In any event, there is sufficient uncertainty in spray production rates, and transport over the waves, as to make the use of more sophisticated formulations of h unnecessary.

FKH estimated that the above parameterization gives the contribution of sea spray to air–sea fluxes comparable to the direct fluxes at wind speeds above 20 m s^{-1} for moisture, and above 35 m s^{-1} for sensible heat. They thus begin to become important at or beyond the point that the HEXOS direct flux measurements end. They also emphasized that this parameterization is valid for wind speeds up to 30 m s^{-1}, but, being based on physically reasonable extrapolations, could be reasonable for wind speeds up to 40 m s^{-1}. In our experiment discussed in the next section, we cut the wind speed off at 32 m s^{-1}, and they are applied with $u_{10} = 32$ m s^{-1} whenever u_{10} exceeds this in (3). This cutoff was implemented so that it is consistent with the second spray parameterization scheme (next subsection), which was validated within this wind speed.

With the effects of sea spray evaporation included, the total air–sea fluxes of sensible and latent heat in the model with this parameterization become

$$H_{S,T} = H_S + Q_{SF} - Q_{LF} \quad \text{and} \quad H_{L,T} = H_L + Q_{LF}, \quad (7)$$

where H_S and H_L are the direct surface sensible and latent heat fluxes. Note that in this equation the feedback factor, 0.5, has been included in the definition of Q_{SF} and Q_{LF}. Clearly the impact of sea spray on the total air–sea enthalpy flux from this parameterization is simply to increase it by Q_{SF}.

c. The Andreas and DeCosmo parameterization

Andreas and DeCosmo (1999) present a parameterization of spray-mediated thermodynamic air–sea fluxes. Two forms are presented, relying on the Andreas (1992) and Andreas (1998) source functions; here we restrict our attention to the latter since it is valid for a wider range of wind speeds. Both are the result of statistical fits of spray-mediated and direct fluxes to the HEXOS heat and moisture flux dataset (DeCosmo et al. 1996). The spray-mediated fluxes are calculated from the droplet evaporation model of Andreas (1992), modified to include a ventilation factor to account for the effects of airflow past a droplet in increasing its evaporation rate, after FKH. The direct fluxes are calculated from the COARE direct flux algorithm (Fairall et al. 1996). They give the total sensible and latent heat fluxes as

$$H_{S,T} = H_S + \beta Q_{\mathrm{SA}} - (\alpha - \gamma) Q_{\mathrm{LA}} \quad \text{and}$$

$$H_{L,T} = H_L + \alpha Q_{\mathrm{LA}}, \tag{8}$$

where α, β, and γ are obtained from the statistical fit, and Q_{SA} and Q_{LA} are ''nominal fluxes'' obtained from the sea spray microphysical model of Andreas (1989, 1992). Here we have reversed their sign convention for Q_{LA} to conform with that of FKH. Fitted values for these coefficients are $\alpha = 4.3$, $\beta = 6.5$, and $\gamma = 3.8$ if the Andreas (1992) source function is used, and $\alpha = 9.8$, $\beta = 15.0$, and $\gamma = 9.3$ for the Andreas (1998) source function. The differences seem to be due largely to the latter source function being around ⅓ to ½ of the former, depending on the droplet radius. The latter set will be used here as that source function is valid to a higher wind speed, 32 m s^{-1}, than the other.

These equations have two substantial differences with the corresponding equations in FKH. First, the ''feedback coefficients'' α, β, and γ are allowed to exceed 1, while FKH took $\alpha = \beta = 0.5$, $\gamma = 0$ and folded them into their final formulas for Q_{SF} and Q_{LF}. Physically, more heat and moisture end up in the atmosphere than is calculated by the microphysics part of the model. However, given the substantial uncertainties in the sea spray source function, it is not unreasonable to suppose that this may be because the droplet production rate during HEXOS was much higher than either of the Andreas (1992, 1998) source functions predicted. Alternatively, if the droplet residence time was longer than assumed by the Andreas (1992) model, this would increase the latent heat flux. Indeed, Kepert et al. (1999) show that the fall velocity parameterization of residence time used by Andreas is an underestimate, due to the effects of turbulence. A further reason for some difference is that unlike FKH, Andreas and DeCosmo (1999) do not include the effects of ventilation due to the droplets' fall speed in their microphysics model, and thereby underestimate the transfer rates. Thus, having these statistically fitted parameters exceeding 1 could plausibly be a consequence of deficiencies in the microphysical model and is, thus, acceptable.

The second difference is that α and β, which control how much of the spray-mediated flux is ''realized'' above the droplet evaporation layer, were assumed by FKH to be equal, but are here allowed to differ. However, as Q_{SA} is in practice much smaller than Q_{LA}, this will not have a major impact (see discussion below and Fig. 3).

The final difference, the introduction of the γQ_{LA} term, which was not considered by FKH, is considerably more difficult to interpret. This will clearly have a profound effect on the net air–sea energy exchange, since the total enthalpy flux is now $H_S + H_L + \beta Q_{\mathrm{SA}} + \gamma Q_{\mathrm{LA}}$, as compared to $H_S + H_L + Q_{\mathrm{SF}}$ in the FKH parameterization, where β was rolled into the definition of Q_{SF}. The extra term γQ_{LA} is a potentially very large term; for instance Andreas and DeCosmo (1999, Fig. 13.8) give $Q_{\mathrm{LA}} = 560$ W m^{-2} at 30 m s^{-1} with an air temperature of 298 K and relative humidity of 80%, so this term alone will contribute over 5000 W m^{-2}! Physically, while the FKH scheme has the moistening due to spray evaporation balanced by the cooling, the Andreas and DeCosmo scheme allows a substantial imbalance, which they speculate may result from a feedback mechanism due to the near-surface cooling. A weakness of their argument, in our view, is that they do not similarly account for the corresponding near-surface moistening. However, as they do obtain an improved fit between parameterization and data using this approach, it is worthwhile to investigate its impact here.

We would, however, like to emphasize that the γQ_{LA} term is not an attempt to model the process detailed by Andreas and Emanuel (1999), whereby a significant mass of spray droplets reenter the ocean significantly cooler than the air, thereby enhancing the droplet-mediated sensible heat flux. This effect is explicitly incorporated into Q_{SA} increasing it by a factor of 2 or 3 over what would apply if the droplets were assumed to reenter the sea at the air temperature and, thus, contributes typically a few tens of watts per meter squared. In contrast, the much larger γQ_{LA} is introduced on the hypothesis that the feedbacks due to profile adjustment in the presence of spray are different for sensible and latent heat: ''Because the evaporating spray cools the droplet evaporation layer and thereby increases the air–sea temperature difference, we add back some of the latent heat responsible for this cooling as γQ_{LA}. . .. Similarly, the spray latent heat flux moistens the DEL [*sic*] and therefore should decrease the humidity gradient that drives HL [*sic*]. But we need not explicitly account for this feedback . . . because α implicitly includes it.'' (Andreas and DeCosmo 1999). The physical processes causing this feedback are not detailed; rather they rely on the statistical fit of their model to the HEXOS observations to justify the use of a nonzero γ.

Andreas and DeCosmo (1999), in contrast to FKH, do not give a simple closed formula for their scheme's fluxes. Application of their parameterization is thus not

straightforward, but requires knowledge of saline microphysics, integration across a range of droplet initial radii with the source function folded in, and further parameterization of various timescales that are not given in a tractable form. These, in practice, give rise to quite complex and computationally expensive calculations. In order to simplify these, we performed a large number of flux calculations using their full model, then carried out a statistical fit to these. As defined by Andreas (1992), calculating the timescales τ_T and τ_r for droplet temperature adjustment and evaporation requires an expensive full integration of the droplet microphysics equations. For numerical convenience, we parameterized these as

$$\tau_T' = -\frac{T_s - T_{\text{ev}}}{\partial T/\partial t}, \tag{9a}$$

$$\tau_r' = -\frac{r_0 - r_{\text{eq}}}{\partial r/\partial t}\left(1 - \frac{1}{e}\right). \tag{9b}$$

These are estimates of the time required for a droplet to experience $(1 - 1/e)$ of its temperature change from T_s to T_{ev}, and $(1 - 1/e)$ of its radius change from r_0 to r_{eq}, respectively. The droplet cooling rate $-\partial T/\partial t$ is evaluated at the initial temperature T_s and radius r_0; the droplet evaporating temperature T_{ev} is essentially a wet-bulb temperature modified for the effects of salinity and curvature (Kepert 1996; Andreas 1996). The cooling rate is close to proportional to the difference between the droplet temperature and T_{ev}, and so the droplet temperature changes nearly exponentially with time, giving (9a). The radius evolution, however, is more complex. If we integrate the full droplet evaporation equation forward in time, the evaporation rate is nearly constant for the first part of the simulation because as the droplet shrinks, the contrary effects of increasing curvature to increase the evaporation rate, and increasing salinity to decrease it, largely cancel. That these effects act in opposition is apparent from inspection of the radius evolution equation [e.g., Andreas 1995, Eq. (2.1)]; the approximate cancellation is the fortuitous conjunction of some parameter values including seawater salinity, typical droplet radii, typical ambient relative humidity, and seawater surface tension. Thus $\partial r/\partial t$ is nearly constant and r decreases approximately linearly in time, at first. Eventually, provided the relative humidity is above about 75%, the salinity effect dominates and the droplet approaches its equilibrium radius r_{eq}, which is largely a function of the ambient relative humidity. However, the initial approximately linear radius evolution means that (9b), with the evaporation rate $\partial r/\partial t$ evaluated at a radius midway between r_0 and its radius at time τ_r, $[r_0(1 + 1/e) + r_{\text{eq}}(1 - 1/e)]$, is an appropriate estimate of τ_r.

These parameterized timescales are compared with those calculated from integrating the full microphysical

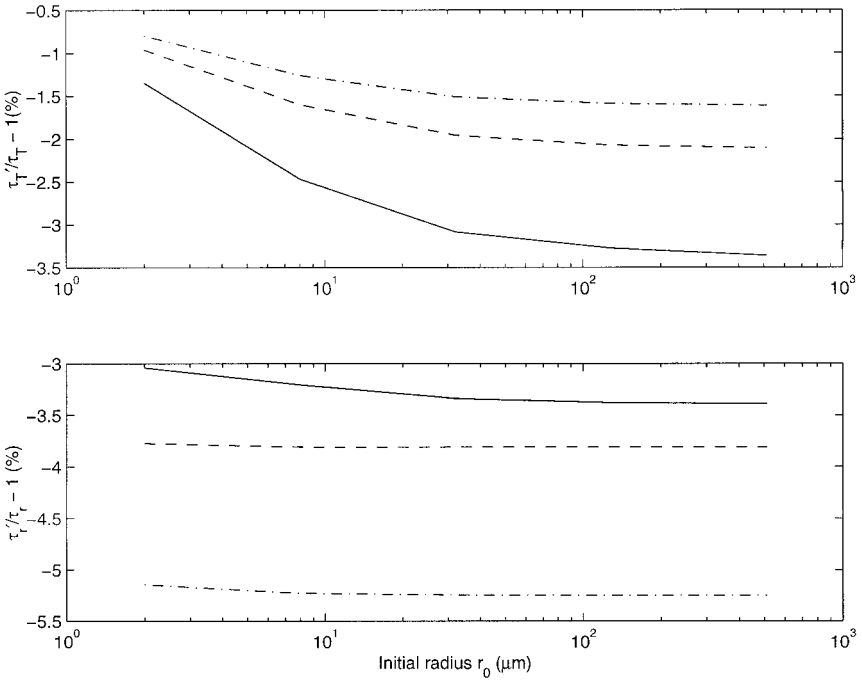

FIG. 2. Percentage differences between (top) droplet sensible and (bottom) latent heat transfer timescales, as defined by Andreas (1992) and calculated from the full microphysical equations, and as parameterized here through Eq. (9), as a function of droplet initial radius. Ambient conditions were $T_s = 300$ K, $T_a = 298$ K, and relative humidity = 80% (solid), 90% (dashed), and 95% (dotted–dashed).

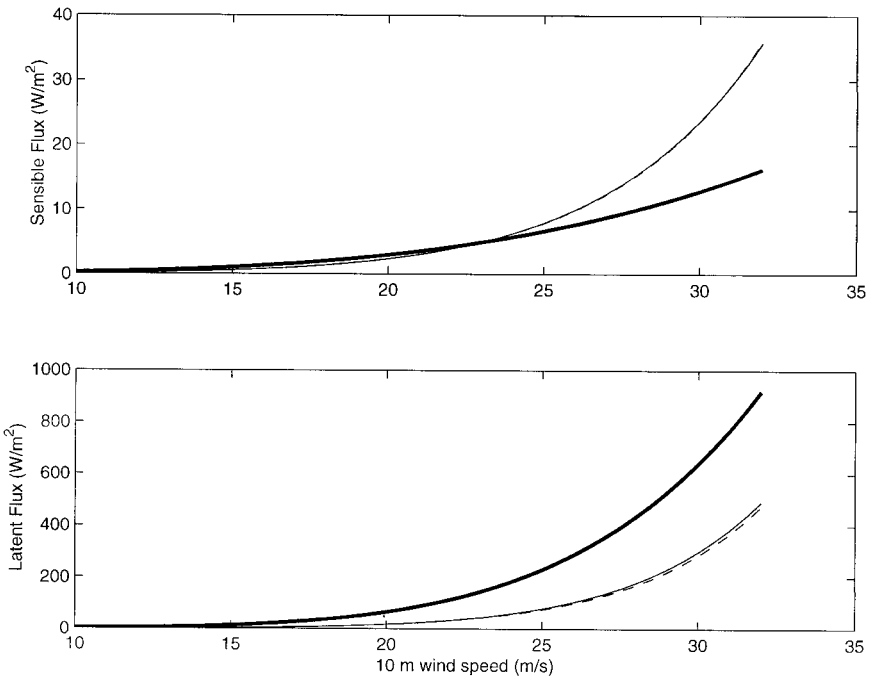

FIG. 3. Spray-mediated (top) sensible and (bottom) latent heat fluxes Q_S and Q_L, without feedback coefficients, according to the parameterization of FKH (heavy solid line), Andreas and DeCosmo (1999) (light solid line), and Andreas and DeCosmo (1999) as simplified here (light dashed line). Other parameters are $T_s = 300$ K, $T_a = 298$ K, and RH = 90%. Before application, these values should be multiplied by the "feedback coefficient" of 0.5 in the case of FKH, or the fitting coefficients $\alpha = 9.8$, $\beta = 15$, and $\gamma = 9.3$ as described in the text in the case of Andreas and DeCosmo.

equations in Fig. 2. For temperature, the parameterized timescale is generally within a few percent of the value calculated from integrating the full microphysical equations forward in time. The agreement for the radius is not quite so good, but is still quite acceptable for our purposes.

We then used Andreas' (1998) model to calculate Q_{SA} and Q_{LA} over a large number (1600) of points spanning the reasonable parameter space for tropical cyclones, which we took to be

$$298 < T_s < 302 \qquad 0.2 < T_s - T_a < 3$$
$$15 < u_{10} < 35 \qquad 0.8 < \text{RH} < 0.96. \quad (10)$$

Statistical fits were then carried out on these parameterized fluxes to derive approximate bulk-type formulas suitable for efficient calculation of the fluxes in our TCM3. The formulas so found were

$$Q_{SA} = 5.309 \times 10^{-8} u_{10}^{5.5191} p(u_{10})(T_s - T_{ev})$$
$$Q_{LA} = 1.853 \times 10^{-5} u_{10}^{6.7893} p(u_{10}) \times (0.98 q_{sat}(T_{ev}) - q)^{0.8274}, \quad (11)$$

where, as in (3), u_{10} is the wind speed at 10 m, T_s is the sea surface temperature, T_{ev} is the droplet evaporating temperature as given in Kepert (1996) or Andreas (1996), and p is a polynomial

$$p(u_{10}) = 0.002431(u_{10} - 23.76)^2 + 0.9242 \quad (12)$$

that incorporates some of the wind speed dependence in the Andreas (1998) source function. These formulas give results that are within 2% for Q_{SA}, and 6% for Q_{LA}, of those calculated from the full Andreas (1992, 1998) model over the parameter range given (Fig. 3), and are thus acceptably accurate for our purposes. Note that the wind speed dependence is different between Q_{SA} and Q_{LA}, because the droplet source function's wind speed dependence varies with radius, and that large droplets are more efficient at transferring sensible rather than latent heat due to the relative timescales.

There are several obvious differences with the FKH parameterization, and the predictions of the two parameterizations for typical tropical cyclone conditions are shown in Fig. 3. Note that the values shown here do not include the effects of the feedback coefficients. First, the wind speed dependence of Q_{LA}, $p(u_{10})u_{10}^{6.7893}$ is stronger than the $u_{10}^{5.4}$ in Q_{LF}. This is largely due to the different source functions used. The wind speed dependence for Q_{SA} is much stronger than for Q_{SF}, as the assumption of FKH that sensible heat transfer occurs instantaneously has been relaxed, and thus an additional u_{10}^2 dependence from the wave height equation enters there. The Q_{SA} equation has $T_s - T_{ev}$ rather than $T_s - T_a$ in Q_{SF}; the latter is typically two to three times small-

er. The $\beta(T_a)$ term in Q_{LF} does not occur in Q_{LA}, since its purpose was to allow the calculation of q_{sat} at T_a rather than T_{ev}, which at the time that FKH developed their parameterization was hard to calculate. As Kepert (1996) and Andreas (1996) give simple formulas for T_{ev}, this is no longer necessary. Finally, the exponent of $\Delta q = [0.98\ q_{sat}(T_{ev}) - q]$ is approximately 0.83, rather than 1. This is at first sight rather counterintuitive; the droplet evaporation rate $\partial r/\partial t$ is very nearly proportional to Δq, and so one might expect the flux to be so also. However, this neglects the fact that the droplets have a nonzero equilibrium radius, at which point they stop evaporating because the increased salinity has suppressed the vapor pressure over their surface. This is a quite nonlinear function of Δq, and some of the smaller droplets, with shorter evaporation timescales and longer residence times, reach or approach this radius. This leads to the dependence of Q_{LA} on Δq not being a direct proportionality. This nonlinear dependence on Δq is also the main reason that the fitted Q_{LA} equation has larger errors than that for Q_{SA}. While a more complex function of Δq would have improved this fit, given the uncertainties inherent in sea spray parameterization, and the need for numerical efficiency, this was deemed to be sufficiently accurate.

Because of the method used in deriving the above formulas, caution should be exercised outside the domain of validity given, although the forms chosen should not give physically unreasonable results for small excursions. However, extrapolation to wind speeds in excess of 32 m s^{-1} should be avoided, since Andreas (1998) states that his source function is invalid past this point. Thus the implementation of these formulas in TCM3 cuts the wind speed off at 32 m s^{-1}, and they are applied with $u_{10} = 32$ m s^{-1} whenever u_{10} exceeds this limit. It is also important to note that the statistical fitting of the Andreas and DeCosmo scheme was based on the COARE algorithm for estimating the interfacial direct fluxes; therefore, the Andreas and DeCosmo parameterization scheme was implemented into our TCM3 with the COARE algorithm for surface direct interfacial flux calculations. The major differences between the two parameterizations, and also the further simplifications introduced by us to the Andreas and DeCosmo (1999) parameterization, are summarized in Table 2.

3. Experimental design

To evaluate the effect of the parameterized sea spray evaporation on tropical cyclone boundary layer structure and intensity, four numerical experiments (Table 3) were conducted. In both experiments E1 and E2, the standard TCM3 algorithm for estimating the surface interfacial fluxes was used. Experiment E1 omitted the effect of sea spray, while E2 utilized the FKH parameterization for sea spray. In experiments E3 and E4, the COARE algorithm (Fairall et al. 1996) was used for interfacial flux calculations. As in E1, E3 omitted the effect of sea spray, while E4 used the streamlined version of the Andreas and DeCosmo (1999) parameterization scheme discussed in section 2c. The model was initialized with an axisymmetric vortex that has the same radial and vertical tangential wind profile as that used in Wang (1999),

$$V_T(r, \sigma) = \begin{cases} \dfrac{3\sqrt{6}}{4} V_m \left(\dfrac{r}{r_m}\right)\left[1 + \dfrac{1}{2}\left(\dfrac{r}{r_m}\right)^2\right]^{-3/2} \sin\left[\dfrac{\pi}{2}\left(\dfrac{\sigma - \sigma_u}{1 - \sigma_u}\right)\right], & \sigma > \sigma_u, \\ 0.0, & \sigma \le \sigma_u, \end{cases} \tag{13}$$

where r denotes radial distance from the vortex center, V_m is the maximum tangential wind at the radius of r_m, and $\sigma_u = 0.1$. The initial vortex has a maximum azimuthal wind of 15 m s^{-1} at a radius of 100 km. Given the wind fields, the mass and thermodynamic fields are obtained based on a nonlinear balance equation so that the vortex satisfies both the hydrostatic and gradient balances (Wang 1995, 1999). To simplify our interpretation of the numerical results, the vortex was embedded on an f plane (18°S) in a quiescent environment, which has a climate mean sounding of September and October at Willis Island, northeast of Australia. The sea surface temperature was fixed at a relatively low value of 26.6°C in order to avoid too strong storms developed in the model so that the validity of the sea spray parameterization schemes discussed in the previous section was not violated considerably. To reduce the effect of spray on the spinup of cumulus convection in the model, we first ran the model with no sea spray for 48 h using the standard TCM3 algorithm. The resultant cyclone then was used as the initial condition for all four of the experiments. The model was integrated for a further 120 h for each experiment. All times given below are measured from the end of the initial 48-h spinup period, that is, when spray is first introduced.

Note that since there have been no observations at very high wind conditions so far that can be used to verify the sea spray source function and some other detailed sea spray microphysics, we do not attempt to explore the effect of sea spray in the whole range of possibility for real tropical cyclones in this study. Bearing this in mind, we recognize that this study is very preliminary and needs to be extended

in the future when data for very high wind conditions from comprehensive observations are available.

4. The numerical results

a. The effects of the FKH parameterization

The evolution of the maximum wind speed at the lowest model level (panel a) and the minimum sea surface pressure (panel b) in the first two experiments is shown in Fig. 4. We can see that inclusion of sea spray evaporation by the FKH parameterization has a moderate effect on the final intensity of the model tropical cyclone. The moderate effect of sea spray on the final intensity of the model tropical cyclone is in contrast to the results of Wang et al. (1999) and Uang (1999) who found that the intensification rate of the model tropical cyclone was reduced by inclusion of sea spray, while the final intensity was little affected.

The difference between the results obtained here and those of Wang et al. (1999) and Uang (1999) was found to be due to the different initial conditions used in those studies. The initial development of convection in the model is dominated by squall-type convection, accompanied by strong downdrafts and downbursts with resultant strong gusty winds near the surface, provided that mixed ice phase microphysics are included (as in all these runs). This squall-type convection propagates outward and then dissipates at large radii in the early stages of the model integration (Wang 1999, 2001). If the sea spray evaporation is included at this spinup stage of the model integration, as was done by Wang et al. (1999) and Uang (1999), the squall-type convection continues for a longer duration as strong outer rainbands, which slows down the intensification of the model tropical cyclone. In this study, we started with an already partially spunup cyclone, in which the initial squall-type convection at large radii had largely dissipated (not shown). As a result, the spinup effect whereby the moistening and cooling from the spray evaporation enhanced the longevity of these outer rainbands was minimized, and there was no significant reduction in the cyclone intensification rate. This early effect from sea spray on intensification rate in the two earlier studies seemed to extend to the lifetime of the model tropical cyclone by developing stronger outer rainbands that played a role in reducing the core convection of a model tropical cyclone. This latter effect apparently diminished the positive feedback due to the presence of sea spray in Wang et al. (1999) and in Uang (1999), while it was largely minimized in our current results. As a result, the final intensity of the model tropical cyclone was moderately increased due to the inclusion of sea spray evaporation.

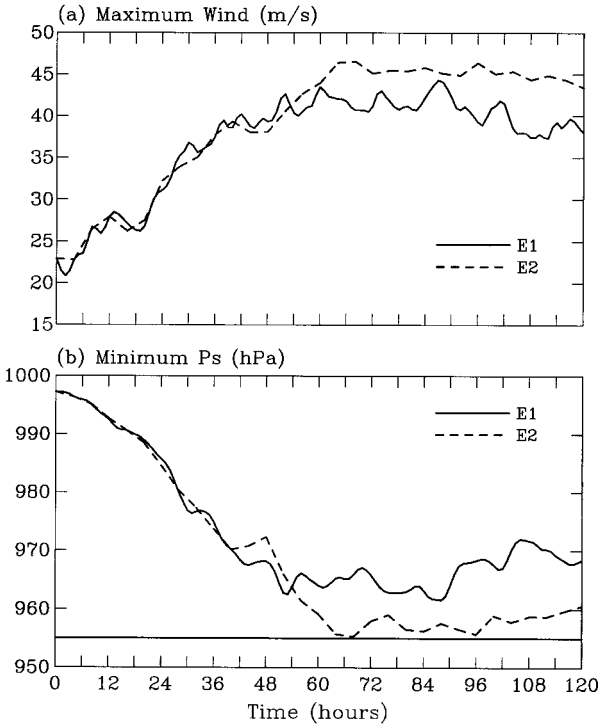

FIG. 4. Evolution of the maximum wind speed (a) at the lowest model level and (b) the minimum sea surface pressure in expts E1 (with no sea spray) and E2 (with FKH's parameterization of spray) based on the standard TCM3 algorithm for direct surface flux calculations, with a fixed sea surface temperature of 26.6°C. The horizontal line shows the maximum potential intensity calculated according to Holland (1997).

The sea spray evaporation parameterized by the FKH scheme modified the boundary layer structure and the activity of convection, and more importantly the direct interfacial fluxes through its effect on the partitioning of the total enthalpy flux into sensible and latent components. Figure 5 compares the azimuthal mean radial distribution of the direct sensible (panel a), latent heat (panel b), and enthalpy (panel c) fluxes in the experiments E1 and E2 during a 6-h mean from 84 to 90 h of time integration. This period was chosen as the cyclone had fully matured, and cyclones in both E1 and E2 were at nearly similar maximum wind speeds (Fig. 4a), reducing the wind speed dependence in comparing fluxes between the storms. Without sea spray, the direct sensible heat flux (thick solid curves) was about 18% of the latent heat flux, or contributed about 15% to the enthalpy flux (defined as latent plus sensible heat fluxes) at the sea surface. This gives a Bowen ratio (sensible heat flux divided by latent heat flux) of about 0.18. With sea spray evaporation, the direct sensible heat flux (thin solid curves) was increased by about 70% (Fig. 5a), while the direct latent heat flux was little changed except for a small increase under the eyewall between 20 and 40 km from the cyclone center (Fig. 5b). As a result, the direct enthalpy flux was increased by about 20% (Fig. 5c) in the near-core region (defined within a radius of 60 km). The Bowen ratio (without the sea spray contribution) in this case increased to about 0.28, which is within the range (0.2–0.3) of previous studies in tropical

TABLE 2. Summary of the main features of the different sea spray parameterization considered here.

	Fairall et al.	Andreas and DeCosmo	Simplified Andreas and DeCosmo
Source function	Modified Andreas (1992)	Andreas (1992) or Andreas (1998)	Andreas (1998)
Temperature evolution	Instantaneous to T_a	Exponential to T_{ev}, timescale from full equation	Exponential to T_{ev}, timescale parameterized
Radius evolution	Linear (with correction for small drops reaching equilibrium)	Exponential to r_{eq}, timescale from full equation	Exponential to r_{eq}, timescale parameterized
Ventilation factor	Included	Omitted	Omitted
Feedback from profile adjustment	Same for heat and moisture, assumed 0.5 on physical grounds	Different for heat and moisture, constants obtained from statistical fit	Different for heat and moisture, constants obtained from statistical fit
Integration over droplet radii	Simplified	Explicit	Incorporated into statistical fit

cyclones (e.g., Frank 1977; Moss and Rosenthal 1975; Black and Holland 1995).

The latent heat flux associated with evaporation of sea spray was about 60%–70% of the direct latent heat flux in the experiment E2 (Fig. 5b). This large latent heat flux produced a loss of sensible heat flux with a magnitude of more than the direct sensible heat flux from the sea surface (Fig. 5a), and an increase in total latent heat flux near the eyewall region by about 50% of that in the experiment without sea spray. The increase in latent heat flux due to evaporation of sea spray resulted in larger rainfall in the cyclone core in experiment E2 than in E1 (Fig. 6). The sensible heat flux due to sea spray itself was only about 6% of the direct sensible heat flux. The net enthalpy flux in E2 due to both direct surface flux and sea spray then was increased by over 20% under the eyewall compared to that in the experiment E1 (Fig. 5c). This is the major reason why the model tropical cyclone was about 8% stronger in maximum wind speed and about 7 hPa deeper in minimum surface pressure in E2 than that in E1 (Fig. 4).

Note that the contribution by the sea spray evaporation [Q_{SF} in (3)] to the total enthalpy flux was less than 1.5% (dashed curve in Fig. 5a). This cannot account for the moderate increase in the model tropical cyclone intensity. Emanuel (1995a) speculated that the sea spray would not affect the maximum achievable intensity of a tropical cyclone as it does not significantly affect the enthalpy flux at the sea surface. This seems not to be true since in our simulation although the contribution of sea spray evaporation to the net enthalpy flux was small, the direct interfacial enthalpy flux was increased due to evaporation of sea spray, which cools the boundary layer, causing an increase in the air–sea temperature difference. We will show later that this latter effect in turn slightly enhanced the buoyancy production of turbulence in the surface layer and, thus, caused a small increase in the interfacial exchange coefficients and finally the enthalpy flux. An interesting result (Fig. 4) is that the model tropical cyclone with the effect of sea spray reached the theoretical MPI developed by Holland (1997). Although this result was obtained by

TABLE 3. Summary of numerical experiments.

Expt	Direct surface flux calculation	Sea spray
E1	TCM3 algorithm	No
E2	TCM3 algorithm	Fairall et al. (1994) parameterization
E3	COARE algorithm	No
E4	COARE algorithm	Streamlined Andreas and DeCosmo (1999) parameterization

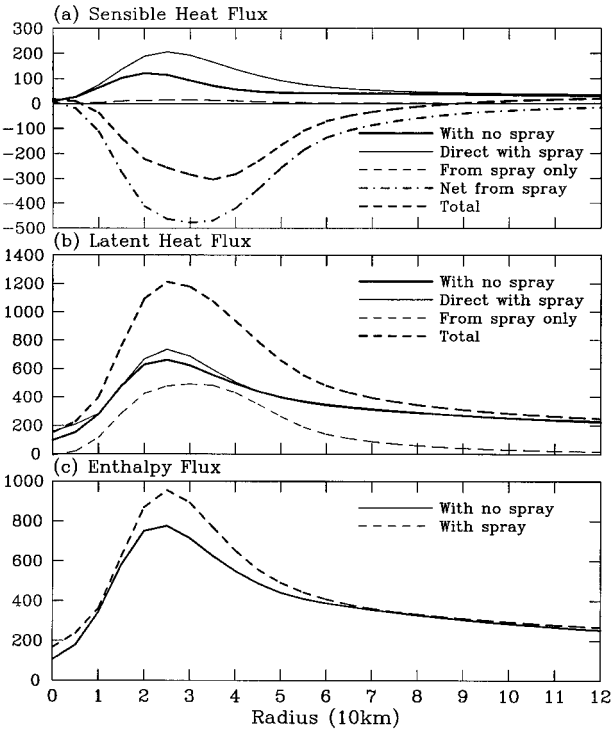

FIG. 5. Radial distribution of the azimuthally averaged (a) sensible and (b) latent heat fluxes, and (c) the enthalpy flux in expts E1 and E2 during a 6-h mean from 84 to 90 h of time integration. Direct fluxes (H_S, H_L), solid; fluxes due to sea spray only (Q_{SF}, Q_{LF}), thin dashed; net sensible heat flux from spray ($Q_{SF} - Q_{LF}$), dotted—dashed; and total heat fluxes ($H_{S,T}$, $H_{L,T}$), thick dashed. The unit in all panels is W m^{-2}.

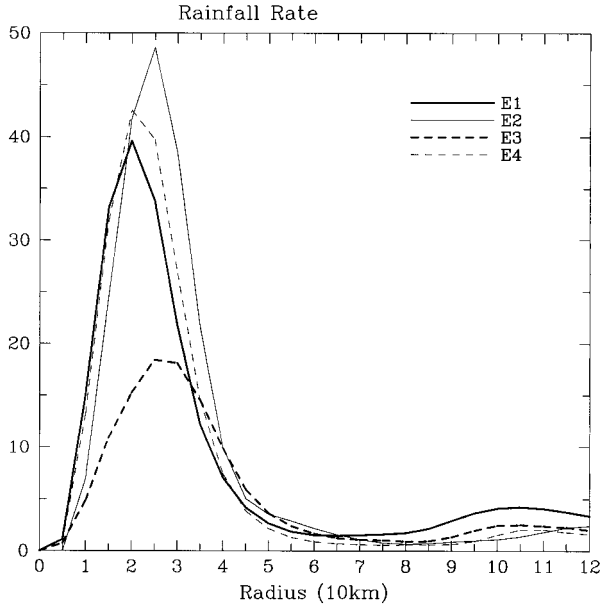

FIG. 6. Radial distribution of rainfall (unit, mm day^{-1}) between 84 and 90 h of time integration in the four experiments listed in Table 3.

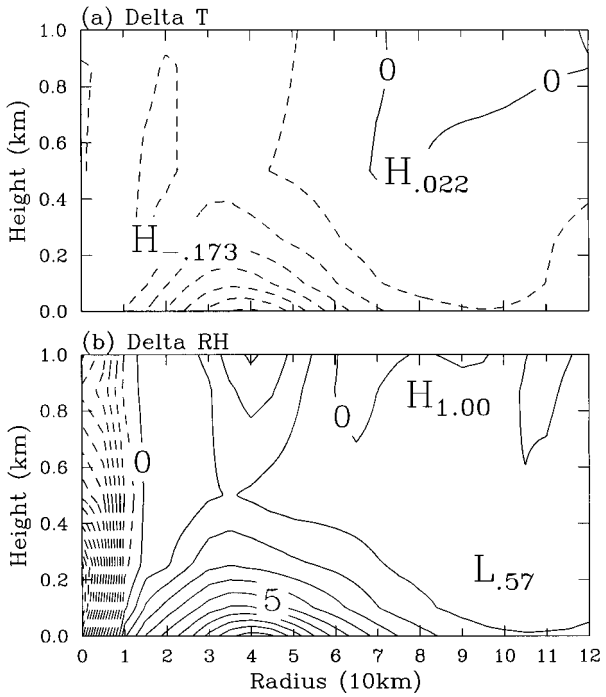

FIG. 7. Radial–vertical cross section of the (a) boundary layer temperature and (b) relative humidity differences (E2 − E1) between the two azimuthal mean cyclones with (E1) and without (E2) sea spray evaporation during a 6-h mean from 84 to 90 h. Contour intervals are 0.2°C for temperature difference, and 1% for relative humidity difference, with the negative values dashed.

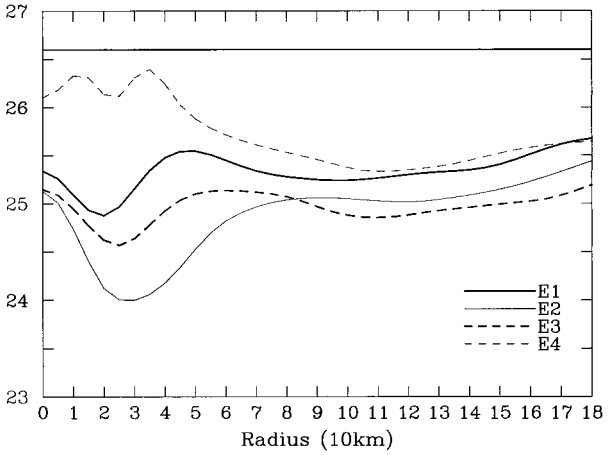

FIG. 8. Radial profiles of azimuthally averaged air temperature (unit, °C) at the lowest model level for all four experiments listed in Table 3 during a 6-h mean from 84 to 90 h. The sea surface temperature is 26.6°C, and is indicated by the horizontal line.

chance, it demonstrates that sea spray evaporation should be included in numerical models in order to predict accurately the intensity of tropical cyclones.

We now examine the physical processes by which the sea spray modifies the boundary layer structure and contributes to the moderate increase in the cyclone intensity. It was indicated above that although the net contribution by sea spray to the total enthalpy flux at the sea surface was small, both the direct interfacial enthalpy flux and the boundary layer structure were modified by the surface layer cooling due to sea spray evaporation. Figure 7 shows the radial–vertical cross sections of the temperature (panel a) and relative humidity (panel b) dif-

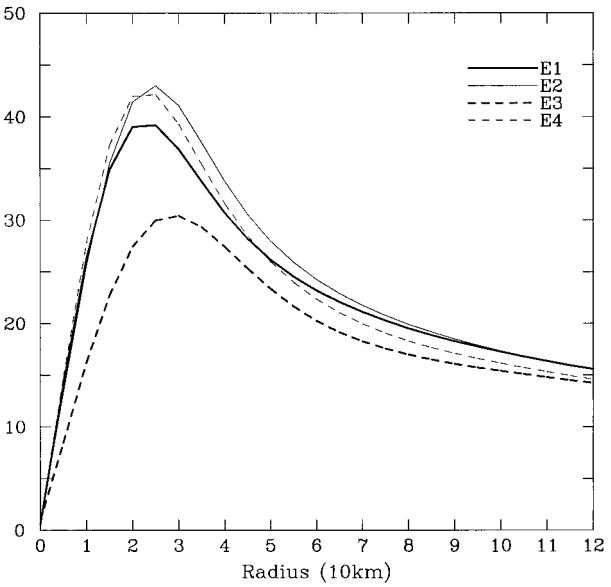

FIG. 9. Radial profiles of azimuthally averaged wind speed (unit, m s^{-1}) at the lowest model level for all four experiments listed in Table 3 during a 6-h mean from 84 to 90 h.

ferences between the two azimuthal mean cyclones with and without the sea spray evaporation (E2 minus E1) during a 6-hourly mean from 84 to 90 h. In agreement with the findings of FKH, with sea spray evaporation, the lower planetary boundary layer was cooler (Fig. 7a) but moister (Fig. 7b). The boundary layer cooling due to sea spray evaporation was maximum (1.4°C) under and just outside the eyewall (which was around 40-km radius), which extended up to 1000 m above the sea surface in the eyewall region and up to 400 m outside the eyewall (Fig. 7a).

The radial profiles of the 6-hourly (between 84 and 90 h) azimuthal mean air temperature at the lowest model level (26.5 m above the sea surface) are shown in Fig. 8, together with the sea surface temperature, which is indicated by the horizontal line at temperature 26.6°C. In experiment E1 (thick, solid curve in Fig. 8), the air temperature is cooler than the sea surface temperature by about 1°C with a small increase in magnitude around 20-km radius, which was due to the evaporation of rain, where the rainfall was maximum (thick, solid curve in Fig. 6). However, in E2 with sea spray evaporation, the air temperature was lower than the sea surface temperature by more than 2.5°C at around 30-km radius and extended to large radii (thin, solid curve in Fig. 8). Although evaporation of rain had a contribution to this larger cooling, it can only partly explain the cooling within a radius of about 50 km since beyond this distance the rainfall was quite small (thin, solid curve in Fig. 6). The major contribution to the cooling, however, was the evaporation of sea spray, which extended to relatively larger radii where the wind speed was above about 15 m s^{-1} (see Figs. 5 and 9). It should be pointed out that adiabatic cooling of the inflow air in the boundary layer had little contribution to the difference of the boundary layer cooling between experiments E1 and E2 shown in Fig. 8. Our estimate showed that the adiabatic cooling due to the pressure drop of the inflow air only can explain a 0.1°C difference in the low-level air temperature between E1 and E2 (not shown). Therefore, evaporation of sea spray by the FKH parameterization scheme played a key role in cooling the tropical cyclone boundary layer. The magnitude of cooling in E2 is consistent with the observational studies of Korolev et al. (1990) and Cione et al. (2000), although we did not find the high magnitudes of cooling found by the former authors. However, our model produces a sharp dip in air temperature right at the radius of maximum winds, partially as a result of rain evaporation. This is in contrast to Cione et al. (2000) who emphasized that the air temperature was nearly constant inside of 150-km radius. The possible explanation for this difference is that current observations could not resolve the cyclone eyewall structure, and thus cooling near the radius of maximum wind in real tropical cyclones could not be seen from current observational dataset.

The cooling in the boundary layer has two potential effects. On the one hand, it can increase the static stability in the lower troposphere, and thus suppress eyewall convection, possibly reducing the tropical cyclone intensity. On the other hand, the increase in air–sea temperature difference may destabilize the surface layer and thus might increase the buoyancy production of the surface-layer turbulence (see Liu et al. 1979), supporting the deep eyewall convection and increasing the cyclone intensity. The former effect seems to play a second role in our simulated tropical cyclone since the convection in the eyewall was mechanically forced rather than convectively driven especially in the mature stage (Emanuel 1986; Zhang et al. 2000). Under this circumstance, moisture flux from both the ocean surface and evaporating sea spray was transported upward by mechanically driven updrafts in the eyewall that tilted outward with height (Fig. 10), especially in E2 with sea spray, which has a more stable stratification within the cyclone core than in E1 (Fig. 7a). Comparing Fig. 10a

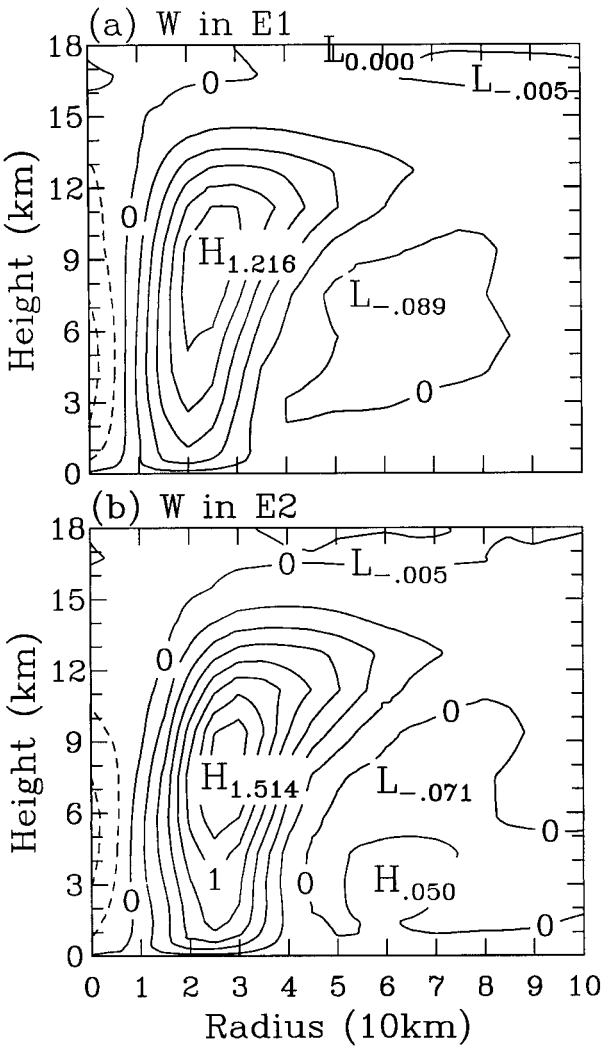

FIG. 10. Radial–vertical cross section of azimuthal mean vertical motion (unit, 1 m s^{-1}) with a contour interval of 0.2 m s^{-1} during a 6-hourly mean from 84 to 90 h in expts (a) E1 and (b) E2.

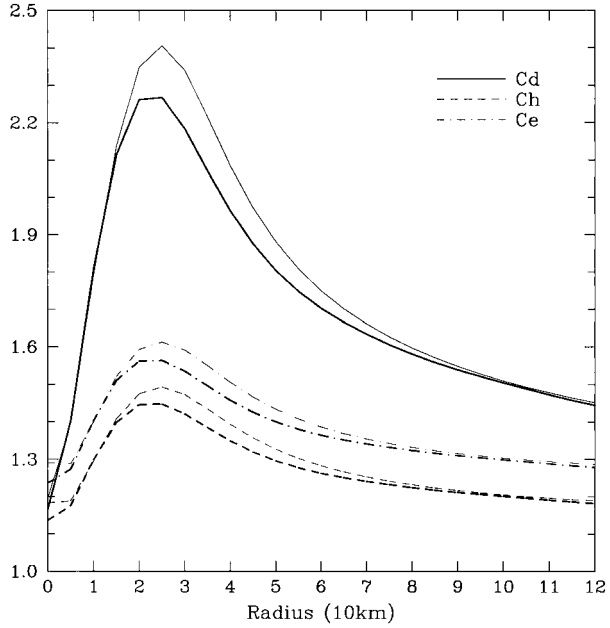

FIG. 11. Azimuthally averaged radial profiles of Cd, Ch, Ce during a 6-h mean from 84 to 90 h in expts E1 (thick) and E2 (thin).

with 10b, one can see that the azimuthally mean eyewall updraft was stronger and tilted more outward with height in E2 than in E1, while the maximum updraft in E2 was lower than that in E1, indicating a slantwise eyewall convection. Since the tropical cyclone boundary layer is believed to be dominated by mechanical turbulence (high wind conditions), the buoyancy-driven turbulence, the second effect of the boundary layer cooling indicated above, should be insignificant. We compared in Fig. 11 the azimuthally mean drag (Cd: solid) and exchange coefficients (Ch: dashed and Ce: dotted–dashed) in experiments E1 (thick) and E2 (thin) for the same time period mean as in Figs. 5–10. Our calculations (not shown) indicated that the difference between the three coefficients in E1 and E2 was mainly due to the increase in wind speeds (Fig. 9), while only about 1% was directly caused by the buoyancy effect (air–sea temperature difference). Therefore, by using the FKH parameterization scheme, sea spray evaporation increases the moisture flux from the surface layer. The increased moisture is transported upward by forced convection in the eyewall and condenses as latent heat in the mid-to upper troposphere, warming the air column and lowering the surface pressure. These consequent events contribute to a moderate increase in model tropical cyclone intensity.

Sea spray evaporation modifies the surface balance toward a cooler and moister boundary layer and, thus, may indirectly affect the boundary layer turbulent flux budget. Such an effect is elucidated in Fig. 12, which shows the vertical divergences of azimuthal mean sensible heat flux (top panels), latent heat flux (middle panels), and enthalpy flux (bottom panels) averaged between 84 and 90 h in both experiments E1 (Fig. 12a, left panels) and E2 (Fig. 12b, right panels). We can see that the boundary layer was warmed by the vertical turbulence mixing with a maximum warming in the eyewall that tilted outward with height (top panel in Fig. 12a). The vertical turbulent mixing only produced moistening (latent heat flux convergence) just within the radius of maximum wind with an exception of drying (latent heat flux divergence) in the lowest layer within 10-km radius (middle panel in Fig. 12a). Drying occurred in a relatively large portion (below 600 m) in the boundary layer from the radius of maximum wind to a radius of about 60 km, where the upward latent heat flux increases with height. The total heat flux (sensible and latent heat fluxes), or enthalpy flux (bottom panel in Fig. 12a), was generally convergent in the eyewall region by turbulence vertical mixing with maximum convergence at the lowest atmosphere, indicating a greater upward enthalpy flux at the sea surface except near the surface in the eye.

When spray evaporation was included, there was a sensible heat flux divergence under and just outside the eyewall in the lowest 40 m from the sea surface (top panel in Fig. 12b), due to a net downward sensible heat flux caused by evaporation of sea spray. Although the net surface sensible heat flux was downward (Fig. 5), the sensible heat flux was still convergent even at the lower levels except for the lowest 40 m under the eyewall. This indicates that a substantial downward heat flux occurred in the boundary layer. This is consistent with both observational studies (Frank 1977; Moss and Rosenthal 1975; Black and Holland 1995) and numerical simulations of tropical cyclones (Kurihara 1975; Anthes and Chang 1978). The drying in the boundary layer due to vertical mixing was increased slightly under the eyewall, and moistening in the inner side of the eyewall was largely enhanced due to the evaporation of sea spray (middle panel in Fig. 12b). However, the total enthalpy flux divergence was little changed with sea spray evaporation (bottom panels in Fig. 12), which mainly occurred in the lower portion of the boundary layer in the eyewall in both cases, indicating that turbulence in the two experiments may be at a similar level in the boundary layer.

b. The effects of the Andreas and DeCosmo parameterization

The time series of maximum wind and central pressure for experiments E3, with the COARE algorithm for surface layer calculation with no spray, and E4, with the Andreas and DeCosmo (1999) spray parameterization, are shown in Fig. 13. We see that the cyclone intensity in E3 was extremely weak, mainly due to the fact that the exchange coefficients produced by the COARE algorithm was too small (Fig. 1) and thus could not support strong tropical cyclones (Emanuel 1995b). The cyclone in E4, however, was much more intense

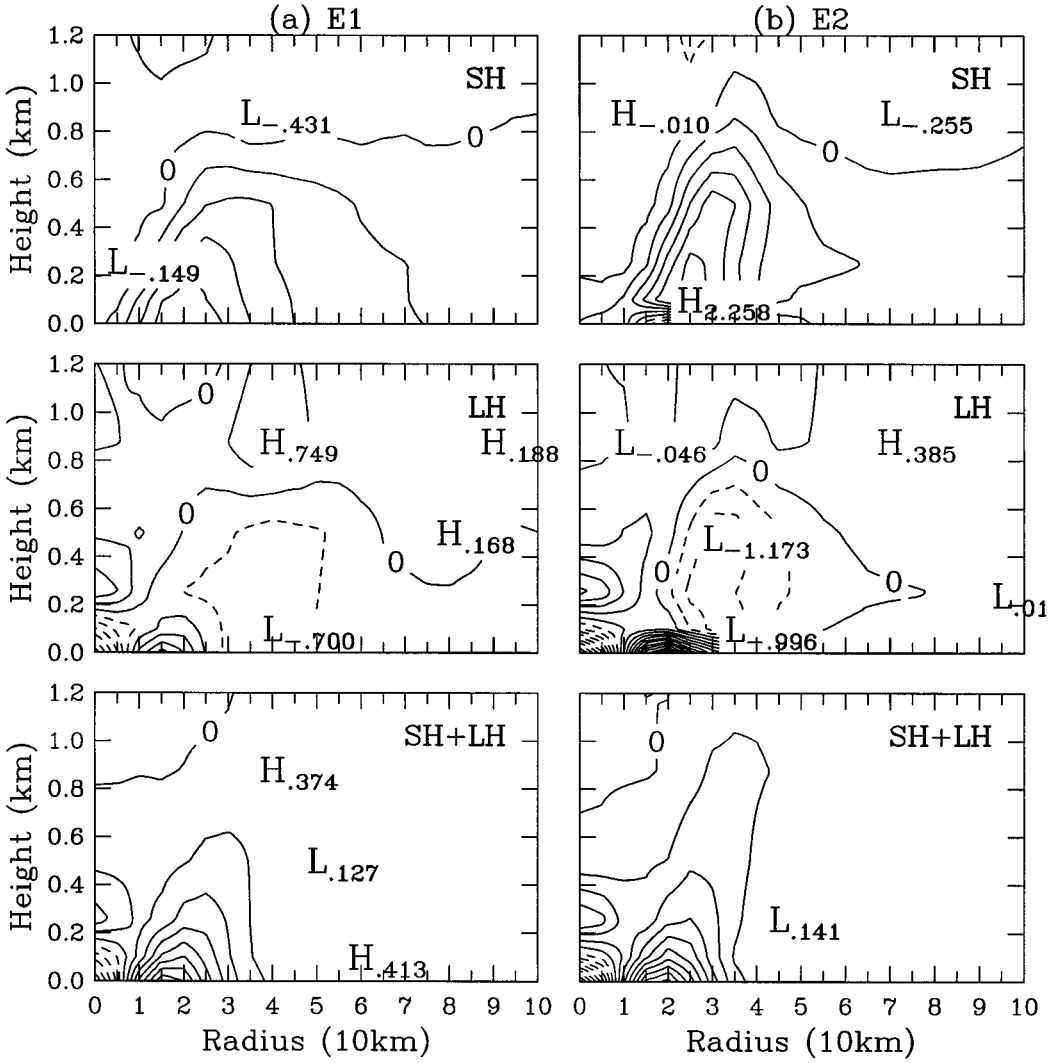

FIG. 12. Radial–vertical cross section of the azimuthally averaged (top) vertical sensible heat, (middle) latent heat, and (bottom) enthalpy flux divergences during a 6-h mean from 84 to 90 h in expts (a) E1 and (b) E2. The unit is W m^{-3}. Contour interval is 0.4 W m^{-3} with negative values dashed.

than in E3, over 10 m s^{-1} in maximum wind, or 19 hPa deeper, reaching a similar final intensity to the cyclone in E3, just by chance. Given the earlier discussion, it is not hard to find reasons for such a remarkable effect of sea spray on the cyclone intensity with the Andreas and DeCosmo (1999) parameterization scheme. They parameterized Q_{LA} in such a way that it is no longer acts as a purely wet-bulb process, but instead contributes substantially to the total enthalpy. Moreover, they also found Q_{SA} to be larger than FKH at high wind speeds, even before being multiplied by their $\beta = 15$ (Fig. 3). This substantial addition to the net enthalpy flux easily accounts for the greater intensity. How large the fluxes have become is shown in Fig. 14, which shows the azimuthal mean radial distribution of the flux components as shown in Fig. 5 for E1, and E2 with the FKH parameterization. Surprisingly, in this case sea spray contributes an upward sensible heat flux close to the total latent heat flux toward the atmosphere (Figs. 14a,b), instead of a net loss of sensible heat of the near surface air discussed above for the FKH parameterization (Fig. 5). This net upward sensible heat flux warms the air near the surface and results in a near-isothermal surface layer in a relatively large area (Fig. 8), which is not supported by any of the available observations (Korolev et al. 1990; Cione et al. 2000), and thus, in our view, is unrealistic. The net enthalpy flux in E4 (Fig. 14c), however, is comparable to that in E2. This explains a similar final tropical cyclone intensity in the two experiments (Figs. 4 and 13).

The direct subsequence of the strong net upward sensible heat flux near the sea surface was to destabilize the boundary layer of the model tropical cyclone, which led to the development of stronger boundary layer tur-

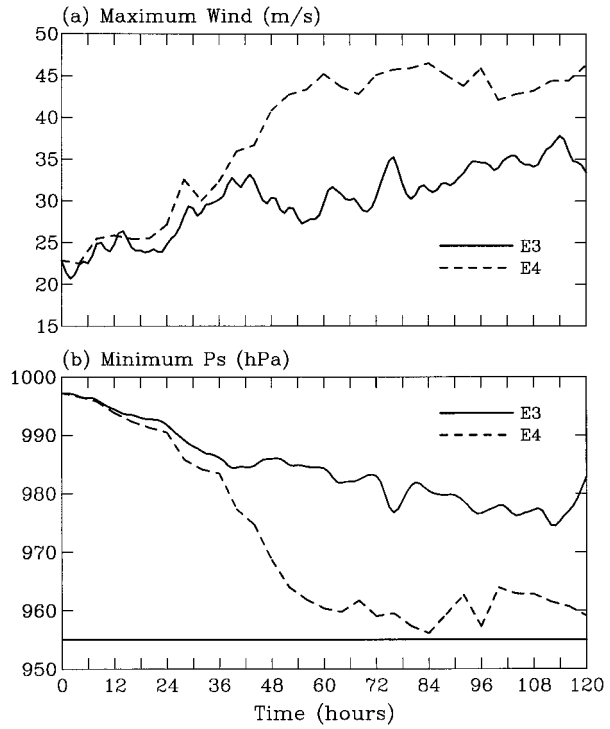

FIG. 13. As in Fig. 4 but for expts E3 (with no sea spray) and E4 (with the streamlined Andreas and DeCosmo parameterization of sea spray), with the COARE algorithm for surface flux calculations (Table 3).

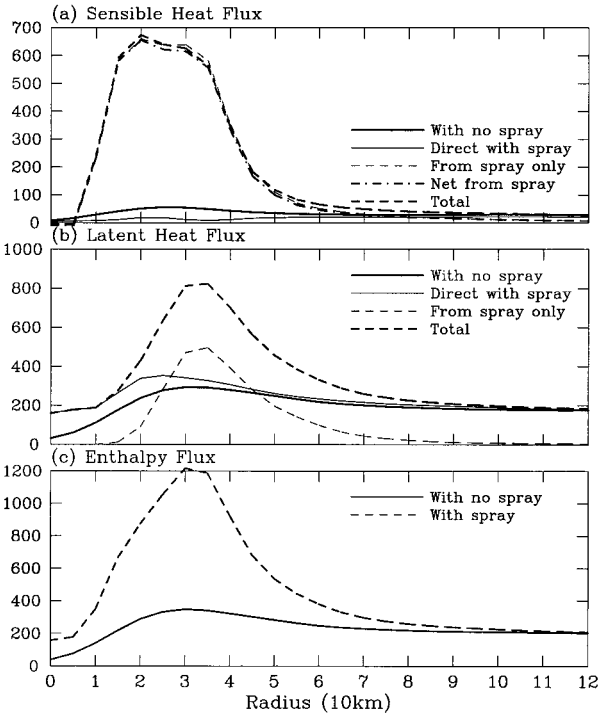

FIG. 14. Radial distribution of the azimuthally averaged (a) sensible and (b) latent heat fluxes and (c) the enthalpy flux in expts E3 (with no spray) and E4 (with the streamlined Andreas and DeCosmo spray parameterization; Tables 2 and 3) during a 6-h mean from 84 to 90 h of time integration. Direct fluxes (H_S, H_L), solid; fluxes due to sea spray only (βQ_{SA}, αQ_{LA}), thin dashed; net sensible flux from spray [$\beta Q_{SA} - (\alpha - \gamma)Q_{LA}$], dotted-dashed; and total heat fluxes ($H_{S,T}$, $H_{L,T}$), thick dashed.

bulence, and vertical turbulent mixing, which is shown in Fig. 15. Although the overall structure of the sensible, latent, and enthalpy fluxes in E3 (Fig. 15a) is similar to that in E1 shown in Fig. 12a, with no sea spray effect, a substantial difference occurred between E2 and E4 (Figs. 12b and 15b), each with the sea spray effect but by different sea spray parameterization schemes. In experiment E4 with the Andreas and DeCosmo parameterization scheme, there was a large sensible heat flux convergence throughout the boundary layer (top panel in Fig. 15b) due to a net upward sensible heat flux and the resultant less stable boundary layer. However, there was a large latent heat flux divergence in the lower levels in E4 (middle panel in Fig. 15b) although the total latent heat flux from the surface and sea spray was large (Fig. 14b), indicating that a strong upward latent heat flux occurred in the boundary layer due to stronger turbulent mixing processes. In contrast to the FKH parameterization scheme used in E2, the sea spray with the Andreas and DeCosmo scheme in E4 substantially contributes to the enthalpy flux convergence throughout the boundary layer (bottom panel in Fig. 15b). This supports deep convection in the eyewall, as seen from the azimuthal mean vertical motion shown in Fig. 16. The vertical motion in E4 (Fig. 16b) was much stronger with a maximum at a higher level in the vertical than that in E3 (Fig. 16a). On the other hand, the maximum vertical motion in E4 was also higher than that in E2 (Fig. 10b), indicating that eyewall convection was more convectively driven in E4 than in E3 due to the less stable stratification in the core region in the former than in the latter.

Although the tropical cyclone intensity in E4 is close to the theoretical maximum potential intensity of Holland (1997), we argue that this might be a result of the unphysical nature of the sea spray parameterization. Certainly, further evidence is needed before we reject the Andreas and DeCosmo parameterization, and our one simulation is just an indication that improvement of the parameterization is required. For instance, possible feedbacks among other physical parameterizations triggered by the extra moisture could play a role. In support of this, we note several explicit droplet dispersion and evaporation modeling efforts (Rouault et al. 1991; Edson and Fairall 1994; Edson et al. 1996; Kepert et al. 1999) that have shown negative feedbacks more like those included in the FKH parameterization, than those included by Andreas and DeCosmo. On the other hand, in its favor is its ability to provide an improved fit to the HEXOS data. However, the fit was based on the COARE algorithm for direct interfacial flux calculations that has been verified for wind speeds only up

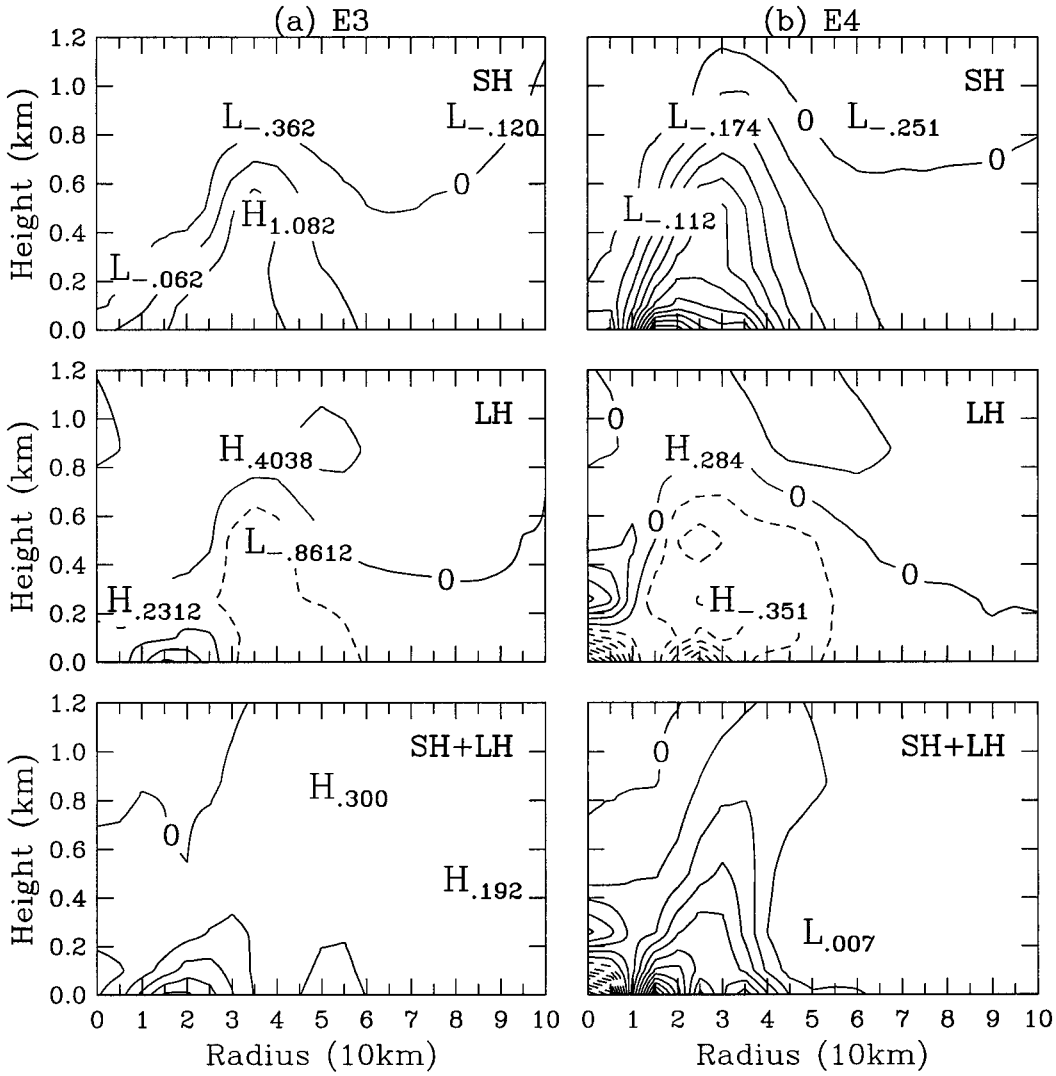

FIG. 15. As in Fig. 12 but for expts (a) E3 and (b) E4 listed in Table 3.

to 14 m s^{-1} (Fairall et al. 1996) and is not necessarily suitable for intense tropical cyclones.

5. Conclusions and discussion

The energy exchange with the ocean is crucial for tropical cyclone development. Given the large amount of sea spray produced by breaking waves at high wind speeds, it is natural to ask whether this alters the air–sea energy transfer sufficiently to affect the intensity or structure of the tropical cyclone. Several earlier studies have considered this question, with varying results. Andreas and Emanuel (1999) found an increase, Wang et al. (1999) and Uang (1999) found no significant change, and Lighthill et al. (1994) and Henderson-Sellers et al. (1998) argued for a decrease. In this paper, a high-resolution tropical cyclone model with explicit cloud microphysics developed by Wang (1999) is used to investigate such a potential effect with the use of two bulk parameterizations for spray-mediated fluxes in consistent model settings.

Using the parameterization of Fairall et al. (1994), our numerical results clearly show that although the net contribution by the sea spray evaporation to the total enthalpy flux was less than 1.5%, cooling due to the sea spray evaporation does indirectly increase the direct interfacial enthalpy flux by about 20%. Consistent with this, the intensity of the model tropical cyclone was moderately increased (8% increase in maximum wind speed) by introduction of sea spray evaporation. This increase in cyclone intensity by sea spray evaporation seems to be in agreement with the results of Andreas and Emanuel (1999), but for quite different physical reasons. In the Fairall et al. parameterization, sea spray affects the intensity of the tropical cyclone by cooling the surface layer, which indirectly enhances the direct

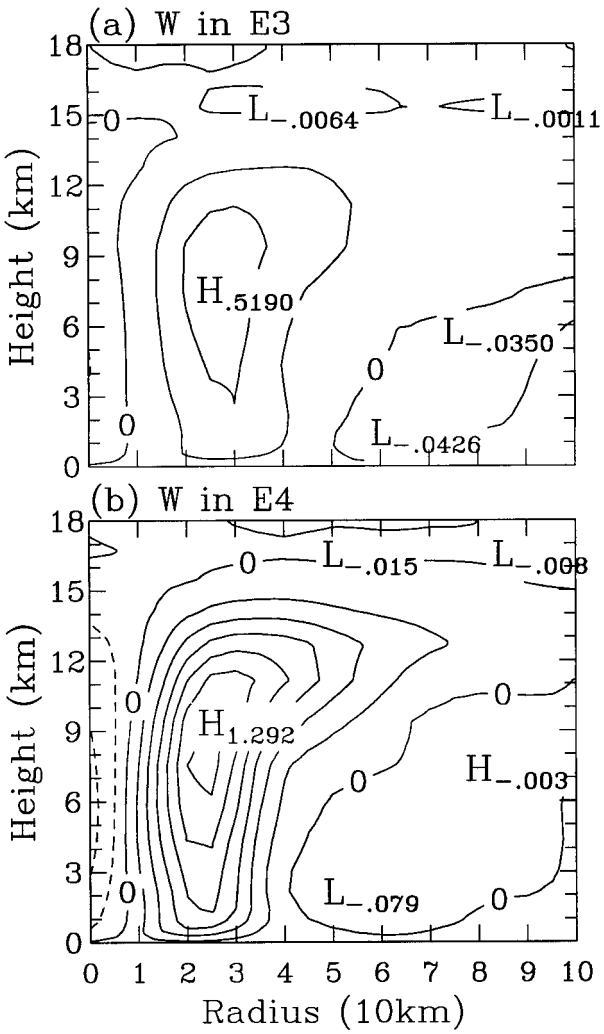

FIG. 16. As in Fig. 11 but for expts (a) E3 and (b) E4 listed in Table 3.

enthalpy flux while doing little to the total enthalpy flux by sea spray itself. However, sea spray in the Andreas and DeCosmo (1999) parameterization directly contributes to the total enthalpy flux and thus increases the cyclone intensity, as is the case in Andreas and Emanuel (1999).

Emanuel (1995a) speculated that the sea spray would not affect the maximum intensity of a tropical cyclone because it does not significantly affect the enthalpy flux at the sea surface. This seems not to be the case. In our simulation although the contribution by sea spray evaporation to the net enthalpy flux was small, the direct interfacial enthalpy flux was increased due to evaporation of sea spray, which cools the boundary layer, causing an increase in the air–sea temperature difference. This latter effect in turn slightly enhanced the buoyancy production of turbulence in the surface layer and, thus, caused a small increase in the interfacial exchange coefficients and finally the total enthalpy flux. Although in this case, the cooling may stabilize the boundary layer just above the surface layer, and thus suppress the eyewall convection and weaken the cyclone, this effect was secondary as the eyewall convection is most likely mechanically forced rather than convectively driven, especially during the mature stage. Although the fact that the model tropical cyclone with sea spray reached the theoretical maximum potential intensity (by both sea spray parameterization schemes) was obtained by chance, it demonstrates that the effect of sea spray evaporation should be included in numerical models in order to predict accurately the intensity of tropical cyclones.

The parameterization of Andreas and DeCosmo (1999) has a marked impact, resulting in the model tropical cyclone being significantly stronger (increased in the maximum wind by 25%) than the one with no spray effect. This is because in this parameterization spray evaporation is not simply a wet-bulb process leaving equivalent potential unchanged, but rather contributes directly to the net enthalpy flux. It also predicts a larger sensible heat flux carried by the droplets than the FKH's parameterization does, producing an unrealistic isothermal surface layer within the model tropical cyclone core region.

As indicated earlier, Andreas and DeCosmo have the advantage of their demonstrated improved fit to the HEXOS observations, against which is the apparently unphysical nature of the feedback parameterization necessary to achieve this fit, while Fairall et al. (1994) conform more closely to the results of explicit droplet modeling efforts. Given that our results, especially for the boundary layer structure, depend strongly on the choice of parameterization, and that the competing choices each have points in their favor, perhaps our firmest conclusion is that further research is needed to determine which most reliably represents reality, as to whether spray would cool or warm the surface layer under a tropical cyclone.

Finally, bearing in mind the uncertainties in the spray parameterization and the available measurements for low wind speed conditions, we reiterate that our study is very preliminary. While it has demonstrated the current understanding of spray physics and the potential impact of sea spray on tropical cyclones, and also exposed several weaknesses that need to be addressed in future studies, it is also necessary to extend the validity of both the spray parameterizations and the algorithm for direct surface flux calculations to very high wind conditions.

Acknowledgments. The authors are grateful to Dr. Edgar Andreas for clarification of the Andreas and DeCosmo (1999) spray parameterization used in this study, and to two anonymous reviewers for their helpful comments on the manuscript. Part of this study has been supported by the Office of Naval Research under Grant ONR-00014-97-001155. The first author has also been

supported partly by the Frontier Research System for Global Change through the International Pacific Research Center at the School of Ocean and Earth Science and Technology of the University of Hawaii. The second author acknowledges useful and stimulating discussions with Chris Fairall.

REFERENCES

Andreas, E. L, 1989: Thermal and size evolution of sea spray droplets. CRREL Rep. 89–11, U.S. Army Cold Regions Research and Engineering Laboratory, Hanover, NH, 37 pp.

——, 1992: Sea spray and the turbulent air–sea heat fluxes. *J. Geophys. Res.,* **97C,** 11 429–11 441.

——, 1995: The temperature of evaporating sea spray droplets. *J. Atmos. Sci.,* **52,** 852–862.

——, 1996: Reply. *J. Atmos. Sci.,* **53,** 1642–1645.

——, 1998: A new sea spray generation function for wind speeds up to 32 m s^{-1}. *J. Phys. Oceanogr.,* **28,** 2175–2184.

——, and J. DeCosmo, 1999: Sea spray production and influence on air–sea heat and moisture fluxes over the open ocean. *Air–Sea Exchange: Physics, Chemistry and Dynamics,* G. L. Geernaert, Ed., Kluwer, 327–362.

——, and K. A. Emanuel, 1999: Effects of sea spray on tropical cyclone intensity. Preprints, *23d Conf. on Hurricanes and Tropical Meteorology,* Dallas, TX, Amer. Meteor. Soc., 22–25.

——, J. B. Edson, E. C. Monahan, M. P. Rouault, and S. D. Smith, 1995: The spray contribution to net evaporation from the sea: A review of recent progress. *Bound.-Layer Meteor.,* **72,** 3–52.

Anthes, R. A., 1982: *Tropical Cyclones. Their Evolution, Structure and Effects. Meteor. Monogr.,* No. 41, Amer. Meteor. Soc., 208 pp.

——, and S. W. Chang, 1978: Response of the hurricane boundary layer to changes of sea-surface temperature in a numerical model. *J. Atmos. Sci.,* **35,** 1240–1255.

Bao, J.-W., J. Wilczak, J.-K. Choi, and L. Kantha, 2000: Numerical simulation of air–sea interaction under high wind conditions using a coupled model: A study of hurricane development. *Mon. Wea. Rev.,* **128,** 2190–2210.

Betts, A. K., and J. Simpson, 1987: Thermodynamic budget diagrams for the hurricane subcloud layer. *J. Atmos. Sci.,* **44,** 842–849.

Black, P. G., and G. J. Holland, 1995: The boundary layer of Tropical Cyclone Kerry (1979). *Mon. Wea. Rev.,* **123,** 2007–2028.

Charnock, H., 1955: Wind stress on a water surface. *Quart. J. Roy. Meteor. Soc.,* **81,** 639–640.

Cione, J. J., P. G. Black, and S. H. Houston, 2000: Surface observations in the hurricane environment. *Mon. Wea. Rev.,* **128,** 1550–1561.

DeCosmo, J., K. B. Katsaros, S. D. Smith, R. J. Anderson, W. A. Oost, K. Bumke, and H. Chadwick, 1996: Air–sea exchange of water vapor and sensible heat: The Humidity Exchange over the Sea (HEXOS) results. *J. Geophys. Res.,* **101,** 12 001–12 016.

Detering, H. W., and D. Etling, 1985: Application of the E–ϵ turbulence model to the atmospheric boundary layer. *Bound.-Layer Meteor.,* **33,** 113–133.

Durran, D. R., and J. B. Klemp, 1982: On the effects of moisture on the Brunt–Väisälä frequency. *J. Atmos. Sci.,* **39,** 2152–2158.

Edson, J. B., and C. W. Fairall, 1994: Spray droplet modelling 1: Lagrangian model simulation of the turbulent transport of evaporating droplets. *J. Geophys. Res.,* **99C,** 25 295–25 311.

——, S. Anquetin, P. G. Mestayer, and J. F. Sini, 1996: Spray droplet modelling. 2: An interactive Eulerian–Lagrangian model of evaporating spray droplets. *J. Geophys. Res.,* **101,** 1279–1293.

Emanuel, K. A., 1986: An air–sea interaction theory for tropical cyclones. Part I: Steady-state maintenance. *J. Atmos. Sci.,* **43,** 585–604.

——, 1991: The theory of hurricanes. *Annu. Rev. Fluid Mech.,* **23,** 179–196.

——, 1995a: Comments on ''Global climate change and tropical cyclones'': Part I. *Bull. Amer. Meteor. Soc.,* **76,** 2241–2243.

——, 1995b: Sensitivity of tropical cyclones to surface exchange coefficients and a revised steady-state model incorporating eye dynamics. *J. Atmos. Sci.,* **52,** 3969–3976.

Fairall, C. W., J. D. Kepert, and G. J. Holland, 1994: The effect of sea spray on surface energy transports over the ocean. *Global Atmos. Ocean Syst.,* **2,** 121–142.

——, E. F. Bradley, D. P. Rogers, J. B. Edson, and G. S. Young, 1996: Bulk parameterization of air–sea fluxes for Tropical Ocean–Global Atmosphere Coupled Ocean Atmosphere Response Experiment. *J. Geophys. Res.,* **101C,** 3747–3764.

Frank, W. M., 1977: The structure and energetics of the tropical cyclone, II: Dynamics and energetics. *Mon. Wea. Rev.,* **105,** 1136–1150.

Garratt, J. R., 1992: *The Atmospheric Boundary Layer*. Cambridge University Press, 316 pp.

Gunn, K. L. S., and J. S. Marshall, 1958: The distribution with size of aggregate snowflakes. *J. Meteor.,* **15,** 452–461.

Henderson-Sellers, A., and Coauthors, 1998: Tropical cyclones and global climate change: A post-IPCC assessment. *Bull. Amer. Meteor. Soc.,* **79,** 19–38.

Heymsfield, A. J., and L. J. Donner, 1990: A scheme for parameterizing ice-cloud water content in general circulation models. *J. Atmos. Sci.,* **47,** 1865–1877.

Holland, G. J., 1997: The maximum potential intensity of tropical cyclones. *J. Atmos. Sci.,* **54,** 2519–2541.

Holt, T., S. Chang, and S. Raman, 1990: A numerical study of the coastal cyclogenesis in GALE IOP2: Sensitivity to PBL parameterizations. *Mon. Wea. Rev.,* **118,** 234–257.

Huang, C.-Y., and S. Raman, 1991: Numerical simulations of January 28 cold air outbreak during GALE. Part I: The model and sensitivity tests of turbulence closures. *Bound.-Layer Meteor.,* **55,** 381–407.

Ikawa, M., and K. Saito, 1991: Description of a nonhydrostatic model developed at the Forecast Research Department of the MRI. Meteorological Research Institute Tech. Res. Paper 28, 238 pp.

Katsaros, K. B., S. D. Smith, and W. A. Oost, 1987: HEXOS—Humidity Exchange Over the Sea. A program for research on water-vapor and droplet fluxes from sea to air at moderate to high wind speeds. *Bull. Amer. Meteor. Soc.,* **68,** 466–476.

Kepert, J. D., 1996: Comments on ''The temperature of evaporating sea spray droplets.'' *J. Atmos. Sci.,* **53,** 1634–1645.

——, and C. W. Fairall, 1999: On the parameterization of spray fluxes for tropical cyclones. Preprints, *23d Conf. on Hurricanes and Tropical Meteorology,* Dallas, TX, Amer. Meteor. Soc., 145–148.

——, ——, and J. W. Bao, 1999: Modelling the interaction between the atmospheric boundary layer and evaporating sea spray droplets. *Air–Sea Exchange: Physics, Chemistry and Dynamics,* G. L. Geernaert, Ed., Kluwer.

Kinsman, B., 1965: *Wind Waves.* Prentice-Hall, 676 pp.

Korolev, V. S., S. A. Petrichenko, and V. D. Pudov, 1990: Heat and moisture exchange between the ocean and atmosphere in Tropical Storms Tess and Skip. *Sov. Meteor. Hydrol.,* **3,** 92–94.

Kurihara, Y., 1975: Budget analysis of a tropical cyclone simulated in an axisymmetric numerical model. *J. Atmos. Sci.,* **32,** 1232–1240.

——, R. E. Tuleya, and M. A. Bender, 1998: The GFDL hurricane prediction system and its performance in the 1995 hurricane season. *Mon. Wea. Rev.,* **126,** 1306–1322.

Langland, R. H., and C.-S. Liou, 1996: Implementation of an *E*–ϵ parameterization of vertical subgrid-scale mixing in a regional model. *Mon. Wea. Rev.,* **124,** 905–918.

Large, W. G., and S. Pond, 1982: Sensible and latent heat flux measurements over the ocean. *J. Phys. Oceanogr.,* **12,** 464–482.

Lighthill, J., G. Holland, W. Gray, C. Landsea, G. Craig, J. Evans, Y. Kurihara, and C. Guard, 1994: Global climate change and tropical cyclones. *Bull. Amer. Meteor. Soc.,* **75,** 2147–2157.

Lilly, D. K., 1964: Numerical solutions for the shape-preserving two-

dimensional thermal convection element. *J. Atmos. Sci.*, **21,** 83–98.
Lin, Y. L., R. D. Farley, and H. D. Orville, 1983: Bulk parameterization of the snow field in a cloud model. *J. Climate Appl. Meteor.*, **22,** 1065–1092.
Ling, S. C., and T. W. Kao, 1976: Parameterization of the moisture and heat transfer process over the ocean under whitecap sea states. *J. Phys. Oceanogr.,* **6,** 306–315.
Liu, T., K. B. Katsaros, and J. A. Businger, 1979: Bulk parameterization of air–sea exchanges of heat and water vapor including the molecular constraints at the interface. *J. Atmos. Sci.,* **36,** 1722–1735.
Marshall, J. S., and W. M. Palmer, 1948: The distribution of raindrops with size. *J. Meteor.*, **5,** 165–166.
Mestayer, P. G., A. M. J. Van Eijk, G. De Leeuw, and B. Tranchant, 1996: Numerical simulation of the dynamics of sea spray over the waves. *J. Geophys. Res.*, **101,** 20 771–20 797.
Miller, M. J., A. C. M. Beljaars, and T. N. Palmer, 1992: The sensitivity of the ECMWF model to the parameterization of evaporation from the tropical oceans. *J. Climate,* **5,** 418–434.
Moss, M. S., and S. L. Rosenthal, 1975: On the estimation of planetary boundary layer variables in mature hurricanes. *Mon. Wea. Rev.,* **103,** 980–988.
Pudov, V. D., and G. J. Holland, 1994: Typhoons and ocean: Results of experimental investigations. BMRC Research Rep. 45, 50 pp. [Available from Bureau of Meteorology Research Centre, Melbourne, Victoria 3001, Australia.]
Reisner, J., R. M. Rasmussen, and R. T. Bruintjes, 1998: Explicit forecasting of supercooled liquid water in winter storms using the MM5 mesoscale model. *Quart. J. Roy. Meteor. Soc.*, **124,** 1071–1107.
Rouault, M. P., P. G. Mestayer, and R. Schiestel, 1991: A model of evaporating spray droplet dispersion. *J. Geophys. Res.*, **96,** 7181–7200.
Rutledge, S. A., and P. V. Hobbs, 1983: The mesoscale and microscale structure and organization of clouds and precipitation in midlatitude cyclones. VIII: A model for the ''seeder-feeder'' process in warm-frontal rainbands. *J. Atmos. Sci.*, **40,** 1185–1206.
——, and ——, 1984: The mesoscale and microscale structure and organization of clouds and precipitation in midlatitude cyclones. XII: A diagnostic modeling study of precipitation development in narrow cold-frontal rainbands. *J. Atmos. Sci.,* **41,** 2949–2972.
Smith, S. D., 1988: Coefficients for sea surface wind stress, heat, and wind profiles as a function of wind speed and temperature. *J. Geophys. Res.*, **93,** 15 467–15 472.
Tripoli, G. J., 1992: An explicit three-dimensional nonhydrostatic numerical simulation of a tropical cyclone. *Meteor. Atmos. Phys.*, **49,** 229–254.
Uang, C.-L., 1999: Impact of sea spray and oceanic response on the development of tropical cyclones. Preprints, *23d Conf. on Hurricanes and Tropical Meteorology*, Dallas, TX, Amer. Meteor. Soc., 30–31.
Wang, Y., 1995: An inverse balance equation in sigma coordinates for model initialization. *Mon. Wea. Rev.,* **123,** 381–401.
——, 1999: A triply-nested movable mesh tropical cyclone model with explicit cloud microphysics. BMRC Research Rep. 74, Bureau of Meteorology Research Centre, 81 pp. [Available from Bureau of Meteorology Research Centre, Melbourne, Victoria 3001, Australia.]
——, 2001: An explicit simulation of tropical cyclones with a triply nested movable mesh primitive equation model: TCM3. Part I: Model description and control experiment. *Mon. Wea. Rev.*, **129,** 1370–1394.
——, J. D. Kepert, and G. J. Holland, 1999: The impact of sea spray evaporation on tropical cyclone intensification. Preprints, *23d Conf. on Hurricanes and Tropical Meteorology,* Dallas, TX, Amer. Meteor. Soc., 26–29.
Zhang, D.-L., Y. Liu, and M. K. Yau, 2000: Multiscale numerical study of Hurricane Andrew (1992). Part III: Dynamically induced vertical motion. *Mon. Wea. Rev.,* **128,** 3772–3788.